Computers and Concrete, *Vol. 26, No. 1* (*2020*) *75-94*
DOI: https://doi.org/10.12989/cac.2020.26.1.075

Free vibration of sandwich micro-beam with porous foam core, GPL layers and piezo-magneto-electric facesheets via NSGT

Mehdi Mohammadimehr*, Saeed Firouzeh, Mahsa Pahlavanzadeh, Yaser Heidari and Mohsen Irani-Rahaghi

Department of Solid Mechanics, Faculty of Mechanical Engineering, University of Kashan, Ghotbe Ravandi Blvd., Kashan, Iran

(*Received April 13, 2020, Revised June 10, 2020, Accepted June 13, 2020*)

Abstract. The aim of this research is to investigate free vibration of a novel five layer Timoshenko microbeam which consists of a transversely flexible porous core made of Al-foam, two graphen platelets (GPL) nanocomposite reinforced layers to enhance the mechanical behavior of the structure as well as two piezo-magneto-electric face sheets layers. This microbeam is subjected to a thermal load and resting on Pasternak's foundation. To accomplish the analysis, constitutive equations of each layer are derived by means of nonlocal strain gradient theory (NSGT) to capture size dependent effects. Then, the Hamilton's principle is employed to obtain the equations of motion for five layer Timoshenko microbeam. They are subsequently solved analytically by applying Navier's method so that discretized governing equations are determined in form of dynamic matrix giving the possibility to gain the natural frequencies of the Timoshenko microbeam. Eventually, after a validation study, the numerical results are presented to study and discuss the influences of various parameters such as nonlocal parameter, strain gradient parameter, aspect ratio, porosity, various volume fraction and distributions of graphene platelets, temperature change and elastic foundation coefficients on natural frequencies of the sandwich microbeam.

Keywords: free vibration; five layers Timoshenko sandwich microbeam; transversely flexible porous core; GPL; piezo-magneto-electric; nonlocal strain gradient theory

1. Introduction

Micro/nano electromechanical systems (MEMS/NEMS) have attracted many researchers in recent years due to their manipulative properties which increases the chance of their application in new classes of high-technology smart electro-mechanical tools. These arrangements can involve various structures, such as composite reinforcements, piezo-magneto-electric skins, elastic foundations, porous materials, etc. The beam structures are somewhat simplest mechanical structures capable of forming single-layer or multi-layer macro, micro and nano devices to demonstrate desired functions.

To study the size effects on the vibration behavior of small-scale structures including micro/nano sandwich beams, many non-classical theories have been suggested through years such as modified couple stress, nonlocal elasticity, strain gradient, modified strain gradient and nonlocal strain gradient theories. Here is a review on some papers which have particularly utilized nonlocal strain gradient theory to perform their analysis. Xiaobai *et al.* (2017) presented bending, buckling and vibration analysis of an axially functionally graded Euler-Bernoulli beam using nonlocal strain gradient theory (NSGT). In their paper, it is concluded that by considering uniformly distributed loads, the maximum deflection with increasing of material length scale parameter decreases because the structure becomes stiffer. Heydari (2018) released his work about vibration and buckling of nanoscale beams chased by a higher order deformation theory. He derived the equations of motion using Eringen's nonlocal theorem and considered accurate position of neutral surface in his formulation. This work introduced new method according to various transform and ways to solve coupled partial differential equations of motion with no simplifications. Free vibration analysis of Euler-Bernoulli nanobeams was conducted by Apuzzo *et al.* (2018) using nonlocal strain gradient theory. In their work, axial and flexural frequencies are investigated for cantilever and fully-clamped nano-beams and influence of nonlocal and strain gradient parameters on fundamental frequencies are studied. Mohammadimehr and Alimirzaei (2016) presented nonlinear static and vibration analysis of Euler-Bernoulli composite beam model reinforced by functionally graded single walled carbon nanotubes with initial geometrical imperfection using finite element method. Also, Ebrahimi and Barati (2017) considered damping vibration characteristics of hygro-thermally affected functionally graded viscoelastic nanobeam. According to results of their paper, the damping ratio (ξ) increases with increasing of nonlocal parameter on the viscoelastic foundation. The governing equations of nonlocal strain gradient viscoelastic are obtained by using Hamilton's principle for different boundary conditions. A size-dependent sinusoidal shear deformation beam model and the free vibration of nanobeams according to the nonlocal strain gradient theory is presented by Lu *et al.* (2017a) that they tried to prove stiff-softening and stiff-

*Corresponding author, Associate Professor
E-mail: mmohammadimehr@kashanu.ac.ir

ISSN: 1598-8198 (Print), 1598-818X (Online)

hardening effects therein. In their article, the governing equations and different boundary conditions are derived by Hamilton's principle and Navier's method is used to find natural frequencies of simply supported nanobeams. Rajabi and Mohammadimehr (2019) studied bending analysis of a micro sandwich skew plate using extended Kantorovich method based on Eshelby-Mori-Tanaka approach. Further, published papers witnessing the recent attitude towards micro/nanobeams analysis through NSGT are those of Liu *et al.* (2019a), Khaniki *et al.* (2018), Li *et al.* (2016), Lu *et al.* (2017b), Sahmani *et al.* (2018c), Şimşek (2019), Xu *et al.* (2017).

The natural composite fillers like sisal fiber (Kumar and Hariharan 2019), $BaTiO_3$@ZnO (Wang *et al.* 2019) or artificial ones like carbon nanotubes/belts (Chan *et al.* 2019, Mohammadimehr and Mostafavifar 2016, Tahouneh 2018), graphene platelets (Javani *et al.* 2019) are used as reinforcement materials that lead to enhance electro-thermo-mechanical performance of structures. Arefi *et al.* (2018a) investigated free vibration behavior of polymer composite nanoplates resting on a Pasternak foundation. In their work, four different FG reinforcement patterns are studied and by using the Halpin–Tsai and the rule of mixture, influence of elastic modulus, the Poisson's ratio and the density of composite nanoplates are investigated. Free and forced vibration of a nanoshell reinforced by graphene platelets (GPLs) was studied by Pourjabari *et al.* (2019). In their paper, three various porosity distributions are analyzed and the novelty of that work is the impact of porosity, GPLRC and MSGT of the nanostructure. Ganapathi *et al.* (2019) examined free vibration and dynamic response of graphene reinforced porous nanocomposite curved beams based on trigonometric shear deformation theory with various types of distributions for porosity. Sobhy (2018) investigated the magneto-electro-thermal bending of doubly-curved shallow shells reinforced by functionally graded graphene platelets surrounded by two piezo-electro-magnetic face sheets with various boundary conditions. From the obtained results, it is concluded that the increase in the GPLs weight fraction and decrease in temperature grow the stiffness of structure. Mohammadimehr *et al.* (2016) depicted size-dependent effect on biaxial and shear nonlinear buckling analysis of nonlocal isotropic and orthotropic micro-plate based on surface stress and modified couple stress theories using differential quadrature method. Kiani and Mirzaei (2019) attempted to excel the researches about graphene platelets reinforcement. Their study stiffened composite laminar plates with thermally influenced nonlinear buckling/post-buckling deformation. Also, an analysis of functionally graded porous micro/nano-beams reinforced with graphene was carried out by Sahmani *et al.* (2018b) with employing a new model for nonlinear bending and the nonlocal strain gradient theory in the third-order shear model for three different porosity distributions along the thickness of structure. In addition, nonlinear free vibration of multilayer functionally graded (FG) porous nanocomposite beams that are made of metal foams and reinforced by GPLs was studied by Chen *et al.* (2017). Free vibration analysis of a functionally graded graphene reinforced porous nanocomposite cylindrical shell was executed by Dong *et al.* (2018) for three kinds of the GPL patterns and four kinds of the porosity distributions. In conclusion section of this study, frequencies of forward and backward and critical spinning speeds for the first order shear deformation theory and the Hamilton's principle are analyzed. Buckling and free vibration of sandwich porous Timoshenko beams with functionally graded (FG) materials were comprehensively discussed by Kitipornchai *et al.* (2017) through the incorporation of Halpin-Tsai model and Ritz solution approach. Yang *et al.* (2018a) presented buckling and free vibration analyses of functionally graded graphene reinforced porous nanocomposite plates with the help of Chebyshev-Ritz solution method. Moradi-Dastjerdi and Bendinan (2019) performed a research about the effect of graphene platelets nanocomposite reinforcement on static and vibrational manner of an axisymmetric cylindrical structure with considerable thickness by application of Halpin-Tsai function. They established that the constitutive materials are temperature dependent. They used a weak form mesh free procedure to extract governing equations. Mohammadimehr *et al.* (2017a) considered nonlinear vibration analysis of functionally graded carbon nanotube reinforced composite for sandwich Timoshenko beam based on modified couple stress theory subjected to longitudinal magnetic field using generalized differential quadrature method. Based on modified strain gradient theory, Mohammadimehr *et al.* (2017b) analyzed dynamic stability of sinusoidal viscoelastic piezoelectric polymeric functionally graded single-walled carbon nanotubes reinforced nanocomposite plate by considering surface stress and agglomeration effects under hydro-thermo-electro-magneto-mechanical loadings. In another research, Yang *et al.* (2017) presented 3D buckling of FG circular and annular plates reinforced by GPLs in thermal environment and solved it analytically by employing Mian and Spencer method. Although, there are already many published articles related to graphene reinforced structures dealing with various mechanical phenomena, like those of Barati *et al.* (2017), Ebrahimi *et al.* (2018), Mirjavadi *et al.* (2019), Reddy *et al.* (2018), Sahmani *et al.* (2018a). Dong *et al.* (2018) studied linear and nonlinear free vibration and dynamic responses of functionally graded graphene platelets reinforced cylindrical shells. Moreover, Dong *et al.* (2019) presented analytical study of graphene platelets reinforced spinning cylindrical shells. In the other work, Dong *et al.* (2020a) analyzed active vibration control of a graphene platelets reinforced cylindrical shell with piezoelectric layers. Also, Dong *et al.* (2020b) worked a research to understand nonlinear resonance behavior of functionally graded graphene platelets cylindrical shells with considering thermal load. Based on linear quadratic regulator (LQR) method, Akhavan Alavi *et al.* (2019) presented active control of micro Reddy beam integrated with functionally graded nanocomposite sensor and actuator. Ghorbanpour Arani *et al.* (2016) illustrated surface stress and agglomeration effects on nonlocal biaxial buckling polymeric nanocomposite plate reinforced by CNT using various approaches.

To study the porosity effect, Kaddari *et al.* (2020)

studied the influence of porosities, aspect ratio and the foundation parameters on bending and vibration of porous FG plate according to a new quasi-3D model. Addou *et al.* (2019) investigated four various patterns of porosity and for evaluation the effect of gradient index, porosity and stiffness parameters, mode numbers of FG plates by using a simple quasi-3D hyperbolic theory. As well as other researcher referred to this new structure such as Medani *et al.* (2019) and Berghouti *et al.* (2019). Ghorbanpour Arani *et al.* (2018) presented a study about rectangular porous plate resting on a Pasternak foundation using Reddy's third-order shear deformation theory. In addition, Ghorbanpour Arani *et al.* (2017) examined free vibration of rectangular plate with porous materials and Reddy's theory was utilized in their paper. Also, Ghorbanpour Arani *et al.* (2019) studied free vibration of sandwich micro-beam by adopting the Euler-Bernoulli beam theory and modified strain gradient theory.

In addition to GPL reinforcement, the technology of piezo-electric, piezo-magnetic as well as piezo-magneto-electric materials have given a new opportunity to convert mechanical deflection to digital signals and vice versa which can be taken for granted in mechanical displacement sensing (Yang *et al.* 2018b), energy harvesting (Liu *et al.* 2019b, Kim *et al.* 2018), and piezoelectric transducers (Qin *et al.* 2019). To achieve this, theoretical studies are required for their characterization. Singh *et al.* (2019) performed a research to understand how a moving load may impact resultant stress components and electric displacements in an irregular transversely isotropic FGPM. To study piezoelectric sandwich nanoplates, Zeng *et al.* (2019) presented the nonlinear vibration of a certain piezoelectric nanoplate with porous core under electrical load. The effects of applied voltage to the piezoelectric layer, distribution and coefficient of porosity on vibration analysis of the sandwich nanoplate were illustrated. Xiong and Tian (2017) analyzed the reaction of FG piezoelectric plates to external time-variant thermal load through the incorporation of finite element methods. In an article by Mahesh *et al.* (2019), frequency response of hydrothermally affected skew magneto-electro-elastic plates was concerned. They suggested Reddy's shear deformation theory for displacement field and adopted Hamilton's energy method for their modeling. Furthermore, Farajpour *et al.* (2019) presented a study over the nonlinear vibration and electromagnetic of magneto-electro-elastic nanofilms under both external electrical voltage and applied magnetic field. The frequency ratio predicted by the nonlocal plate model was greater than that by the classical theory which showed higher positive initial displacements along in-plane directions leading to higher nonlinear buckling voltages. A hyperbolic shear deformation model was conducted by Shokravi (2019) to examine buckling behavior of a multilayer beam with piezoelectricity effects. They utilized differential quadrature (DQ) method to find the dynamic instability region. In another work, free vibration of piezoelectric hollow circular FG-single walled boron nitride nanotubes (SWBNNTs) reinforced nanocomposite plate under action of thermal loadings was analyzed by Mohammadimehr *et al.* (2018) using modified couple stress theory. Bending analysis of a functionally graded shear and normal deformable sandwich nanoplate with piezoelectric face sheets resting on silica aerogel was proposed by Ghorbanpour Arani *et al.* (2019) who have studied free vibration of the configuration as well by means of nonlocal theory (Ghorbanpour Arani *et al.* (2018)). A porous sandwich Timoshenko beam with one-dimensional carbon nanotube (CNT) reinforced piezo-magneto-electric face sheets made of temperature-dependent materials was modeled and examined by Bamdad *et al.* (2019). Also, Amir *et al.* (2018) analyzed the vibration of a porous rectangular plate which was located between two piezo-electro-magnetic layers based on nonlocal elasticity theory. It was observed that by increasing the electric and magnetic potentials, natural frequency decreases and increases, respectively. Moreover, magneto-electro-hygro-thermal buckling of piezoelectric nanoplates was analyzed by Karimiasl *et al.* (2019). They showed that by increasing length scale parameter, natural frequency increases. Another study on piezoelectricity was done by Marzbanrad *et al.* (2017) presenting vibration analysis of an elastically restrained configuration subjected to magneto-thermo-electrical field. They discussed the effect of nonlocal parameter, piezoelectric voltage and magnetic field and length of nanobeam on natural frequencies. Jandaghian *et al.* (2016) studied the free vibration analysis of magneto-electro-thermo-elastic (METE) nanobeams resting on a Pasternak foundation based on nonlocal theory and Timoshenko beam theory. Sheng *et al.* (2013) extended the nonlinear vibration control of cylindrical shells with thin piezoelectric layers based on Hamilton's principle and Von Kármán nonlinear theory. In that work, it is obvious that piezoelectric layers can considerably improve the damping effect of FG cylindrical shells. Among other investigations, Karroubi and Irani-Rahaghi (2019) presented the free vibration analysis of a rotating cylindrical shell with two piezoelectric layers. Ansari *et al.* (2015) studied a geometrically nonlinear beam with different boundary conditions which were solved numerically. In another work, Baroudi and Najar (2019) conducted an analysis on flexoelectric nanobeams including static and dynamic behaviors after extracting governing equations using Hamilton's principle based on Von Karman nonlinear strain field. A number of further reports dealing with piezo-magneto-electricity in mechanics are provided by Arefi *et al.* (2016, 2018, 2019b), Hajmohammad *et al.* (2018), Rostami *et al.* (2019).

There are some published papers related to first-order shear deformation theory (FSDT), higher-order shear deformation theory (HSDT), the elastic foundation, nonlocal strain gradient theory and nonlocal elasticity theory and micro-beams that referred to this paper. By using a simple first-order shear deformation theory (SFSDT), Draiche *et al.* (2019) studied the static analysis of reinforced composite plates. Their results with the conventional FSDT have been compared. Also, Balubaid *et al.* (2019) investigated the different influencing of the vibrational behavior such as the small scale effect, geometry ratio, material index and aspect ratio according to the nonlocal two variables integral. The effect of the

variation of the volume fraction, the power index, Winkler spring constant on the fundamental frequency, center deflection, normal and shear stress of FG-beam resting on the elastic foundation was investigated by Chaabane *et al.* (2019). Hussain *et al.* (2019) analyzed the vibrational frequency of single walled carbon nanotubes (SWCNTs) and by increasing the nonlocal parameter decreases the frequencies based on nonlocal elasticity theory. Different numerical results to show the effect of the variation of the volume fraction, the power index, the slenderness ratio and the influence of Winkler spring constant on the fundamental frequency, center deflection, normal and shear stress of FG-beam was presented by Tlidji *et al.* (2019). Karami *et al.* (2019) examined buckling based on nonlocal strain gradient theory for various boundary conditions using Galerkin's approach. The bending and buckling of nanobeams based on nonlocal strain gradient theory was proposed by Adda Bedia *et al.* (2019).

Thermal effects and porosity are two other assumptions of the present work, which can be found among a huge number of old and new researches as parts of their analyses. In addition to the works mentioned above which contain these two phenomena, Akgoz *et al.* (2018) depicted thermo-elastic vibrational response of microbeams laying on Pasternak's elastic foundation using modified strain gradient theory (MSGT) by considering various beam models. Critical temperature and natural frequencies were reported numerically. A functionally graded nanobeam in thermal environment was the case of Ebrahimi *et al.* (2015) who employed a semi analytical differential transform method for the first time (as they have claimed) and nonlocal elasticity theory to present numerical results.

The novelty of this research can be stated as the combination of aforementioned materials that it yields construction of advices with new performances to fit for the application of interest. It should be remarked that within the numerical results, the effect of temperature is also investigated by assuming temperature-dependent materials and also by considering the effects of applied electric and magnetic potentials, nonlocal parameter, strain gradient parameter, porosity, volume fraction of graphene platelets which can be considered as a novelty. A sandwich Timoshenko beam with a porous transversely flexible core offering a low weight is taken into consideration. The core is embedded in two skins reinforced by GPL nanofillers. The resultant configuration is surrounded by $B_iT_iO_3$-$CoFe_2O_4$ piezo-magneto-electric face sheets able to sense mechanical deformations. The five-layers is laid on Pasternak's foundation and hinged at both ends. As the structure is in a thermal environment, a temperature change is induced through the thickness of every layer which is supposed to be distributed uniformly. Such a configuration is not studied yet and thus is a novel one. In addition to, the novelty of the developed mathematical model is the application of nonlocal strain gradient theory to develop the governing equations with the aid of Hamilton's principle. The governing equations are solved by Navier's method using trigonometric series. Finally, a comprehensive parametric analysis is reported to figure out how various parameters of the system influence its natural frequencies. The examined and discussed parameters include distribution

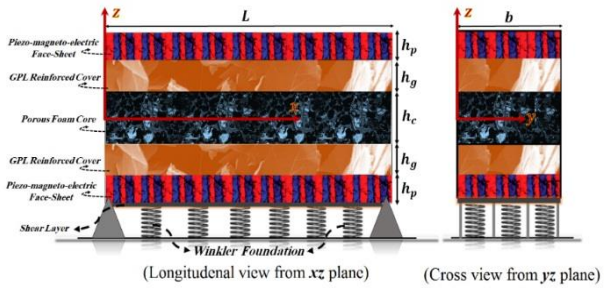

Fig. 1 A schematic view of the five-layers sandwich microbeam

pattern of graphene and porosity, temperature change, porosity coefficient, graphene volume fraction, elastic foundation parameters, wave number, initial applied electric and magnetic potentials and various aspect ratios (such as slenderness, thickness of one layer to thickness of another, etc.). A novel example is proposed in current paper as an attempt to be a benchmark for future technological efforts.

2. Formulation

A sandwich structure with considering piezoelectric and magnetic layers is used as sensor in industrial tools such as aerospace bodies to control vibrations by changing the potential. The use of graphene platelets nanocomposite layers can help these structures to show more efficient application due to their light weight and high strength that is a good capability for aerospace and many other industries. Control process is not the goal of this paper, but the effects of applied electric and magnetic potential on the natural frequency is studied.

The study case of the current work is a sandwich microbeam as depicted in Fig. 1. It consists of a transversely flexible porous foam core covered by GPL facesheets and they are bonded with piezo-magneto-electric face sheets layers.

Here is a list of the basic assumptions that are made for the current formulations.

- The beam structure is modeled based on Timoshenko's theory.
- The beam is at micro scale.
- The stress-strain relations are found through nonlocal strain gradient theory.
- The beam consists of five perfectly bonded layers.
- The vibrations are assumed to be linear.
- The beam is simply supported, i.e., hinged at its endings.
- The core is transversely flexible and has some pores.
- The temperature of the beam is assumed to change with a uniform distribution along the thickness in one case. Also, in another case, it is assumed that the material properties are dependent to temperature.
- The two graphene reinforced layers are established to stiffen the structure.
- The structure rests on a two-variable elastic foundation, one as Winkler coefficient and one as shear layer coefficient.

Table 1 Mechanical properties of Al-FCSB

$E_C^0\ (GPa)$	ν_C^0	$\rho_C^0\ (kg/m^3)$	$\alpha_c\ (10^{-6}K^{-1})$
0.6	0.3	540	20

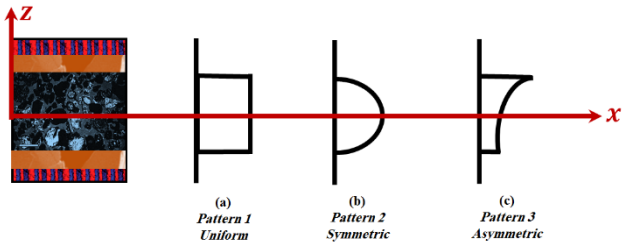

Fig. 2 A schematic view of distribution of porosity in the core

2.1 Characterization of transversely flexible foam core

With the assumption of transversely flexibility, in-plane strain and consequently stress (i.e., *yz* plane) can be neglected due to such a low Young's modulus. Moreover, despite of being desirably light, these materials offer a good mechanical behavior in combination with common composite reinforcements, either mixed or bonded as covers (Adewale *et al.* 2019, Sadighi *et al.* 2011).

Among the available foam materials, Al-FCSB is selected in this work to shape up the core of the sandwich microbeam. Mechanical properties are presented in Table 1 (Mohammadimehr *et al.* 2017).

2.2 Characterization of porosity in transversely flexible core

To study effect of porosity appeared in the core, three common distribution patterns can be considered as depicted in Fig. 2.

Pattern 1 suggests a uniform distribution along the thickness. Patterns 2, 3 illustrate non-uniform distributions. Although Pattern 2 assumes a symmetric distribution with no porosity on the top and bottom surfaces, pattern 3 assumes different amount of porosity on the top and bottom surfaces. Mathematical model of porous core is written as follows (Bamdad *et al.* 2019).

$$E_c(z) = E_c^0(1 - e_0\,\lambda) \tag{1a}$$

$$\rho_c(z) = \rho_c^0\left(1 - \left(1 - \sqrt{1 - e_0}\right)\lambda\right) \tag{1b}$$

$$\nu_c(z) = 0.221\Lambda + \nu_c^0(0.342\Lambda^2 - 1.21\Lambda + 1) \tag{1c}$$

$$\Lambda = 1 - \left(\rho_c(z)/\rho_c^0\right) \tag{1d}$$

where λ is defined according to desirable distribution pattern.

$$\lambda(z) = \frac{1}{e_0} - \frac{1}{e_0}\left(\frac{2}{\pi}\sqrt{1 - e_0} - \frac{2}{\pi} + 1\right)^2 \qquad \text{Pattern 1(2a)}$$

$$\lambda(z) = \cos(\pi z/h_c) \qquad \text{Pattern 2(2a)}$$

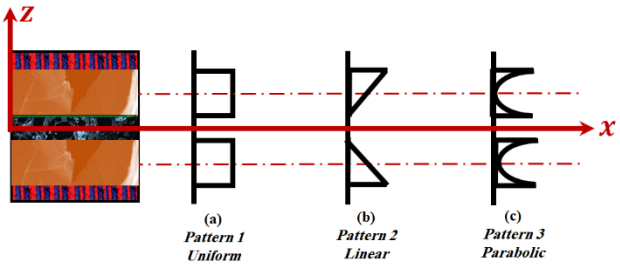

Fig. 3 A various distribution patterns of graphene platelets through polymer matrix in GPL covers

$$\lambda(z) = \cos(\pi z/h_c + \pi/4) \qquad \text{Pattern 3(2a)}$$

in which e_0 is coefficient of porosity and can be written as

$$e_0 = 1 - E_2/E_1 \tag{3}$$

E_1 and E_2 denote maximum and minimum Young's moduli of the porous core, respectively. It can be concluded that range of e_0 is between 0 (no porosity) to less than 1 (almost no foam).

2.3 Characterization of GPL reinforced layers

The core is covered by GPL sheets from top and bottom. The volume fraction of GPL nanofillers can be expressed as (Kitipornchai *et al.* 2017, Yang *et al.* 2018)

$$V_{GPL} = \frac{W_{GPL}}{W_{GPL} + (\rho_{GPL}/\rho_m)(1 - W_{GPL})} \tag{4}$$

pattern of mixing graphene nanofillers within the polymer matrix of GPL covers. Three distribution patterns are recommended in Fig. 3 which can be modeled as a function of GPL covers thickness as the following relations.

According to the Fig. 3(a), a uniform distribution along the thickness for GPL can be modeled as

$$W_{GPL} = \vartheta_1 W_{GPL}^0 \quad \text{for both GPL covers} \tag{5}$$

According to the Fig. 3(b), a linear distribution for graphene's weight fraction along the thickness of GPL covers is expressed as

$$W_{GPL} = \begin{cases} \vartheta_2 W_{GPL}^0\left(\dfrac{z - h_c/2}{h_g}\right) & \text{for the top GPL cover} \\ \vartheta_2 W_{GPL}^0\left(\dfrac{-z - h_c/2}{h_g}\right) & \text{for the bottom GPL cover} \end{cases} \tag{6}$$

Parabolic pattern for weight fraction of nanofillers is depicted in Fig. 3(c) that this distribution offers maximum weight fractions at the upper and the lower surface of top GPL cover and zero in the mid-level of it; however, for the bottom GPL cover, it is the reverse. This pattern is modeled as

$$W_{GPL} = \begin{cases} \vartheta_3 W_{GPL}^0\left(\dfrac{z - (h_c + h_g)/2}{\dfrac{h_g}{2}}\right)^2 & \text{the top GPL cover} \\ \vartheta_3 W_{GPL}^0\left(\dfrac{z + (h_c + h_g)/2}{h_g/2}\right)^2 & \text{the bottom GPL cover} \end{cases} \tag{7}$$

Table 2 GPL indices and weight fraction characteristics

$W_{GPL}^0 = 0\%$	$W_{GPL}^0 = 0.33\%$	$W_{GPL}^0 = 1\%$
0	1/3	1
0	2/3	2
0	1	3

W_{GPL}^0 in Eqs. (5)-(7) is a characteristic value for GPL's weight fraction and determines total percentile content of GPL nanofillers. $\vartheta_1, \vartheta_2 \; and \; \vartheta_3$ denote the weight fraction indices. These parameters are chosen from Table 2.

After specifying volume fraction using Eq. (4), the mechanical properties of GPL covers can be obtained in the following way. Young's modulus of GPL covers considering Halpin-Tsai model (Halpin *et al.* 1976) can be presented as follows.

$$\mathrm{E_g} = \frac{3}{8}\left(\frac{1+\xi_L \Xi_L V_{GPL}}{1-\Xi_L V_{GPL}}\right)E_M + \frac{5}{8}\left(\frac{1+\xi_b \Xi_b V_{GPL}}{1-\Xi_b V_{GPL}}\right)E_M \quad (8a)$$

$$\Xi_L = \frac{E_{GPL}/E_M - 1}{E_{GPL}/E_M + \xi_L} \quad (8b)$$

$$\Xi_b = \frac{E_{GPL}/E_M - 1}{E_{GPL}/E_M + \xi_b} \quad (8c)$$

in which, E_{GPL} and E_M are Young's moduli of GPLs and matrix, respectively. ξ_L and ξ_b denote geometry ratios of GPL covers which are expressed as

$$\xi_L = 2(L/h_g) \quad (9a)$$

$$\xi_b = 2(b/h_g) \quad (9b)$$

Poison's ratio of GPL covers can be obtained by means of the rule of mixture.

$$\nu_g = \nu_{GPL} V_{GPL} + \nu_M (1 - V_{GPL}) \quad (10)$$

in which, ν_{GPL} and ν_M are Poisson ratios of GPL nanofillers and matrix, respectively. Mass density of GPL covers is expressed as

$$\rho_g = \rho_{GPL} V_{GPL} + \rho_M (1 - V_{GPL}) \quad (11)$$

where, ρ_{GPL} and ρ_M denote mass density of nanofillers and polymer matrix, respectively. The thermal expansion coefficient of GPL covers can be written as

$$\alpha_g = \alpha_{GPL} V_{GPL} + \alpha_M (1 - V_{GPL}) \quad (12)$$

α_{GPL} and α_M describe thermal expansion coefficients of graphene nanofillers and matrix, respectively. Values of properties of graphene nanofillers and polymer matrix used to create GPL covers are listed in Table 3.

Table 3 Values of properties of graphene nanofillers and polymer matrix

$E_{GPL}\,(TPa)$	ν_{GPL}	$\rho_{GPL}\,(10^3\,kg/m^3)$	$\alpha_{GPL}\,(10^{-5}K^{-1})$
1.01	0.006	1.06	2.35
$E_M\,(GPa)$	ν_M	$\rho_M\,(10^3\,kg/m^3)$	$\alpha_M\,(10^{-5}K^{-1})$
2.85	0.34	1.2	8.2

2.4 Characterization of piezo-magneto-electric face sheets

As shown in Fig. 1, three layers (i.e., the core and GPL covers) are surrounded by piezo-magneto-electric face sheets.

Basically, equations for piezo-magneto-electric face sheets expressed regarding Maxwell's equations for transversely polarized face sheets (Ansari *et al.* 2015, Arefi *et al.* 2019, Karrubi *et al.* 2019, Sheng *et al.* 2013). Electric vector and magnetic intensity are introduced as

$$\begin{Bmatrix} E \\ H \end{Bmatrix}_j = -\nabla \begin{Bmatrix} \psi \\ \phi \end{Bmatrix}_j \quad (j = tp, bp) \quad (13)$$

where ψ_j and ϕ_j are electric and magnetic potentials, respectively and $\nabla = (\frac{\partial}{\partial x}, \frac{\partial}{\partial z})$.

The electric and magnetic potentials can be obtained in form of linear and cosine functions as

$$\begin{cases} \psi_j(x,z,t) = 2\psi_0 \dfrac{\bar{z}_j}{h_p} - \psi(x,t) cos\left(\dfrac{\pi \bar{z}_j}{h_p}\right) \\ \phi_j(x,z,t) = 2\phi_0 \dfrac{\bar{z}_j}{h_p} - \varphi(x,t) cos\left(\dfrac{\pi \bar{z}_j}{h_p}\right) \end{cases} \quad (14)$$

in which ψ_0 and ϕ_0 denote applied electric and magnetic potentials, respectively, and $\psi(x,t)$ and $\varphi(x,t)$ denote undetermined electric and magnetic potentials, respectively. $\bar{z}_{tp} = z - \frac{h_c + 2h_g + h_p}{2}$ and $\bar{z}_{bp} = z + \frac{h_c + 2h_g + h_p}{2}$ denote z axis translated to geometric mid surface of top and bottom piezo face sheets, respectively.

Eq. (14) into Eq. (13) is written as follows

$$\begin{Bmatrix} E_x \\ E_z \end{Bmatrix}_j = -\begin{Bmatrix} \dfrac{\partial \psi}{\partial x} \\ \dfrac{\partial \psi}{\partial z} \end{Bmatrix}_j = \begin{Bmatrix} \dfrac{\partial \psi}{\partial x} cos\left(\dfrac{\pi \bar{z}_j}{h_p}\right) \\ -2\dfrac{\psi_0}{h_p} - \psi \dfrac{\pi}{h_p} sin\left(\dfrac{\pi \bar{z}_j}{h_p}\right) \end{Bmatrix} \quad (15)$$

And also

$$\begin{Bmatrix} H_x \\ H_z \end{Bmatrix}_j = -\begin{Bmatrix} \dfrac{\partial \Phi}{\partial x} \\ \dfrac{\partial \Phi}{\partial z} \end{Bmatrix}_j = \begin{Bmatrix} \dfrac{\partial \phi}{\partial x} cos\left(\dfrac{\pi \bar{z}_j}{h_p}\right) \\ -2\dfrac{\phi_0}{h_p} - \varphi \dfrac{\pi}{h_p} sin\left(\dfrac{\pi \bar{z}_j}{h_p}\right) \end{Bmatrix} \quad (16)$$

Consequently, electric vector and magnetic intensity are described by Eqs. (15) and (16), respectively, as components in x and z directions. In order to obtain properties of piezo-magneto-electric face sheets to consist with Timoshenko beam model, the presented relation for property coefficients (Jandaghian *et al.* 2016) are utilized here to find those taking place in the present work through the following relations.

$$Q_{11p} = C_{11} - C_{13}^2/C_{33}; \quad Q_{22p} = C_{44};$$
$$e_{113} = e_{31} - C_{13}e_{33}/C_{33}$$
$$e_{311} = e_{113} = e_{31} - C_{13}e_{33}/C_{33} \; ; \; e_{131} = e_{15}; \quad q_{113} = q_{31} - C_{13}q_{33}/C_{33}$$

$$q_{311} = q_{113} = q_{31} - C_{13}q_{33}/C_{33}\ ;\ \ q_{131} = q_{15}\ \ ;\ \ \eta_{11} = s_{11};\ \eta_{33} = s_{33} + e_{33}^2/C_{33}$$
$$g_{11} = d_{11}\ \ ;\ \ g_{33} = d_{33} + q_{33}e_{33}/C_{33}\ ;\ \ \beta_{11} = \mu_{11};\ \ \beta_{33} = \mu_{33} + q_{33}^2/C_{33}$$
$$\rho_p = \rho\ \ ;\ \ \alpha_p = \frac{\lambda_1 - C_{13}\lambda_3/C_{33}}{C_{11} - C_{13}^2/C_{33}} \tag{17}$$

The left side of relations in Eq. (17) are involved parameters in current paper, while the right side parameters are those used in Jandaghian *et al.* (2016).

By substituting given values in Jandaghian *et al.* (2016) into Eq. (17), customized coefficients can be determined as in Table 4.

It should be noted that α_p (thermal expansion coefficient of piezo face sheets) is calculated in terms of the thermal moduli (Jandaghian *et al.* 2016, Sankar *et al.* 2002).

2.5 Governing equations for the sandwich microbeam

Assuming perfect bonding at the interfaces of the current sandwich microbeam, the linear displacement fields for all five layers can be expressed within the framework of Timoshenko beam model as Bamdad *et al.* (2019).

$$U(x,z,t) = u(x,t) + z\theta(x,t) \tag{18a}$$

$$W(x,z,t) = w(x,t) \tag{18b}$$

where u and w denote the axial and transverse displacements respectively and θ is rotation of the cross section about *y*-axis.

The normal and shear strains for Timoshenko micro beam are obtained using Eqs. (18) as follows.

$$\varepsilon_{xx} = \frac{\partial u}{\partial x} + z\frac{\partial \theta}{\partial x} \tag{19a}$$

$$2\varepsilon_{xz} = \Upsilon_{xz} = \theta + \frac{\partial w}{\partial x} \tag{19b}$$

In order to capture size effects including stiff-softening and stiff-hardening, nonlocal strain gradient theory (NSGT) is proposed to obtain constitutive equations of the layers (Arefi *et al.* 2019, Bamdad *et al.* 2019, Lu *et al.* 2017a).

For the transversely flexible porous foam core, constitutive relations based on NSGT are as

$$(1-\epsilon\nabla^2)\begin{Bmatrix} t_{xx} \\ t_{xz} \end{Bmatrix} = (1-\varrho\nabla^2)\begin{bmatrix} Q_{11c} & 0 \\ 0 & k_s Q_{22c} \end{bmatrix}\begin{Bmatrix} \varepsilon_{xx} \\ \Upsilon_{xz} \end{Bmatrix} \tag{20}$$

in which, $\epsilon = (e_0 a)^2$ and $\varrho = l^2$ represent the nonlocal parameter $(e_0 a)$ and the strain gradient parameter (l), respectively. t_{xx} and t_{xz} are the total stress components which are defined in terms of classical stress and the higher order stress as the following form.

$$\begin{Bmatrix} t_{xx} \\ t_{xz} \end{Bmatrix} = \begin{Bmatrix} \sigma_{xx} - \nabla\sigma_{xx}^{(1)} \\ \sigma_{xz} - \nabla\sigma_{xz}^{(1)} \end{Bmatrix} \tag{21}$$

where in Eq. (20), $\nabla^2 = \frac{\partial^2}{\partial x^2}$ is Laplacian operator, k_s is the shear strain correction factor (5/6 for rectangular Timoshenko beam model), Q_{11c} and Q_{22c} denote elastic constants of the core and are described as functions of z direction as follows.

Table 4 Material properties of piezo-magneto electric face sheets ($B_iT_iO_3$-$CoFe_2O_4$)

Property coefficients			
Elastic (GPa)	Q_{11p}=154.81	Q_{22p}=44.2	
Piezo-electric (C/m^2)	e_{113}=-7.54	e_{311}=-7.54	e_{131}=5.8
Piezo-magnetic (N/Am)	q_{113}=89.23	q_{311}=89.23	q_{131}=275
Dielectric (10^{-9} C/Vm)	η_{11}=5.64	η_{33}=6.75	
Magneto-electric (10^{-12} Ns/VC)	g_{11}=5.367	g_{33}=17802.64	
Magnetic permeability (10^{-6} Ns^2/C^2)	β_{11}=-297	β_{33}=84.07	
Mass density (10^3 kg/m^3)	ρ_p=5.55		
Thermal expansion (10^{-6} K^{-1})	α_p=1.38		

$$Q_{11c} = \frac{E_c(z)}{1-\nu_c^2(z)} \tag{22a}$$

$$Q_{22c} = \frac{E_c(z)}{2\left(1+\nu_c(z)\right)} \tag{22b}$$

For the GPL reinforced covers, constitutive equations are expressed as

$$(1-\epsilon\nabla^2)\begin{Bmatrix} t_{xx} \\ t_{xz} \end{Bmatrix} = (1-\varrho\nabla^2)\begin{bmatrix} Q_{11g} & 0 \\ 0 & k_s Q_{22g} \end{bmatrix}\begin{Bmatrix} \varepsilon_{xx} \\ \Upsilon_{xz} \end{Bmatrix} \tag{23}$$

where, Q_{11g} and Q_{22g} are given as

$$Q_{11g} = \frac{E_g(z)}{1-\nu_g^2(z)} \tag{24a}$$

$$Q_{22g} = \frac{E_g(z)}{2\left(1+\nu_g(z)\right)} \tag{24b}$$

Constitutive equations for the piezo-magneto-electric face sheets may seem different from those of the core and GPL covers due to involving magnetic-field-magnetic-intensity as well as electric-displacement-electric-vector relations. These relations can be proposed as follows (Ansari *et al.* 2015, Arefi *et al.* 2019, Bamdad *et al.* 2019, Karrubi *et al.* 2019, Lu *et al.* 2017a).

$$(1-\epsilon\nabla^2)\begin{Bmatrix} t_{xx} \\ t_{xz} \end{Bmatrix} = (1-\varrho\nabla^2)\left(\begin{bmatrix} Q_{11p} & 0 \\ 0 & k_s Q_{22p} \end{bmatrix}\begin{Bmatrix} \varepsilon_{xx} \\ \Upsilon_{xz} \end{Bmatrix} - \begin{bmatrix} 0 & e_{113} \\ e_{131} & 0 \end{bmatrix}\begin{Bmatrix} E_x \\ E_z \end{Bmatrix} - \begin{bmatrix} 0 & q_{113} \\ q_{131} & 0 \end{bmatrix}\begin{Bmatrix} H_x \\ H_z \end{Bmatrix}\right) \tag{25a}$$

$$(1-\epsilon\nabla^2)\begin{Bmatrix} D_x \\ D_z \end{Bmatrix} = (1-\varrho\nabla^2)\left(\begin{bmatrix} 0 & e_{131} \\ e_{311} & 0 \end{bmatrix}\begin{Bmatrix} \varepsilon_{xx} \\ \Upsilon_{xz} \end{Bmatrix} + \begin{bmatrix} \eta_{11} & 0 \\ 0 & \eta_{33} \end{bmatrix}\begin{Bmatrix} E_x \\ E_z \end{Bmatrix} + \begin{bmatrix} g_{11} & 0 \\ 0 & g_{33} \end{bmatrix}\begin{Bmatrix} H_x \\ H_z \end{Bmatrix}\right) \tag{25b}$$

$$(1-\epsilon\nabla^2)\begin{Bmatrix} B_x \\ B_z \end{Bmatrix} = (1-\varrho\nabla^2)\left(\begin{bmatrix} 0 & q_{131} \\ q_{311} & 0 \end{bmatrix}\begin{Bmatrix} \varepsilon_{xx} \\ \Upsilon_{xz} \end{Bmatrix} + \begin{bmatrix} g_{11} & 0 \\ 0 & g_{33} \end{bmatrix}\begin{Bmatrix} E_x \\ E_z \end{Bmatrix} + \begin{bmatrix} \beta_{11} & 0 \\ 0 & \beta_{33} \end{bmatrix}\begin{Bmatrix} H_x \\ H_z \end{Bmatrix}\right) \tag{25c}$$

D_x and D_z are electric displacements in x and z directions, respectively. B_x and B_z denote components of magnetic field in x and z directions, respectively.

The total strain energy of the sandwich microbeam can be formed as the sum of strain energy stored in the face sheets, GPL covers and the core and also energies caused by electric and magnetic fields in piezo-magneto-electric face sheets.

$$\Pi_p = \frac{1}{2}\int ({t_{ij}}^r {\varepsilon_{ij}}^r - {D_x}^j {E_x}^j - {D_z}^j {E_z}^j - {B_x}^j {H_x}^j - {B_z}^j {H_z}^j) dA dz_r \quad (r = c, tg, bg, tp, bp; j = tp, bp) \tag{26}$$

By entering Eqs. (15), (16) and (19) into Eq. (26) and then taking variations, variation of potential energy can be defined as

$$\delta\Pi_p = -\iint [\,(N_{xx,x}\ \delta u + (M_{xx,x} - N_{xz})\delta\theta + N_{xz,x}\delta w - (C_{x,x} + C_z)\delta\psi\ \ -(F_{x,x} + F_z)\delta\varphi]dxdy \tag{27}$$

where

$$\{N_{xx}, M_{xx}, N_{xz}\} = \sum \{{N_{xx}}^r, {M_{xx}}^r, {N_{xz}}^r\} \tag{28}$$

and

$$\{{N_{xx}}^r, {M_{xx}}^r, {N_{xz}}^r = \int \{t_{xx}, t_{xx}\, z, t_{xz}\} dz_r \tag{29}$$

Resultants $C_x, C_z, F_x$and F_z which are associated with energies of piezo face sheets can be written as

$$\{C_x, C_z, F_x, F_z\} = \sum \{{C_x}^j, {C_z}^j, {F_x}^j, {F_z}^j\} \tag{30}$$

where,

$$\{{C_x}^j, {F_x}^j\} = \int \{D_x, B_x\} cos\left(\frac{\pi \bar{z}_j}{h_p}\right) dz_j \tag{31a}$$

$$\{{C_z}^j, {F_z}^j\} = \int \{D_z, B_z\} \frac{\pi}{h_p} sin\left(\frac{\pi \bar{z}_j}{h_p}\right) dz_j \tag{31b}$$

The kinetic energy for each layer can be given by

$$\Pi_k = \frac{1}{2}\int \rho_r (\dot{U}^2 + \dot{W}^2) dA dz_r \tag{32}$$

in which ρ_r indicates mass density of each layer. $\dot{U}$ and $\dot{W}$ are given by

$$\dot{U} = \dot{u}(x,t) + z\dot{\theta}(x,t) \tag{33}$$

$$\dot{W} = \dot{w}(x,t) \tag{34}$$

Inserting Eqs. (33) and (34) into Eq. (32) yields

$$\Pi_k = \frac{1}{2}\iint (I_1\, \dot{u}^2 + I_3\dot{\theta}^2 + I_1\dot{w}^2 + 2I_2\dot{u}\,\dot{\theta}) dxdy \tag{35}$$

in which, I_1 , I_2 and I_3 denote the sum of cross section moments of each layer in the following form.

$$\{I_1, I_2, I_3\} = \sum \{{I_1}^r, {I_2}^r, {I_3}^r\} \tag{36a}$$

$$\{{I_1}^r, {I_2}^r, {I_3}^r\} = \int \rho_r \{1, z, z^2\} dz_r \tag{36b}$$

To substitute the total kinetic energy into Hamilton's principle, its variation is derived as

$$\delta\Pi_k = -\iint [(I_1\, \ddot{u} + I_2\ddot{\theta})\delta u + (I_1\ddot{w})\delta w + (I_3\ddot{\theta} + I_2\ddot{u}\,)\delta\theta\,] dxdy \tag{37}$$

Variation of work done by thermal environmental, applied electric potential and magnetic potential can be modeled as (Akgöz *et al.* 2018, Ebrahimi *et al.* 2015, Wang *et al.* 2019b).

$$\delta\Pi_w = -\iint (N^T + N^E + N^M) w_{,xx}\, \delta w dxdy \tag{38}$$

where, N^T is sum of thermal resultants of each layer and can be written as the following form

$$N^T = \sum \int Q_{11r}\, \alpha_r \Delta T dz_r \tag{39}$$

in which, ΔT denotes temperature change. Note that temperature change can be assumed distributed either uniformly along z-direction or non-uniformly. In this paper, uniform distribution is taken into consideration.

Also, N^E and N^M denote piezoelectric and piezomagnetic resultants, respectively, as follows.

$$N^E = -\frac{2}{h_p}\int e_{113}\, \psi_0 dz_j \ ; \ N^M = -\frac{2}{h_p}\int q_{113}\, \phi_0 dz_j \tag{40}$$

Variation of work done by Pasternak's foundation can be obtained by Mohammadimehr *et al.* (2010)

$$\delta\Pi_{wF} = \iint (-K_1 w + K_2 w_{,xx})\delta w\, dxdy \tag{41}$$

in which, K_1 and K_2 are Winkler and shear layer coefficients, respectively.

Finally, substituting of Eqs. (27), (37), (38) and (41) into Hamilton's principle $\int \delta(\Pi_k - \Pi_p + \Pi_w + \Pi_{wF})\, dt = 0$, leads to obtain the equations of motion in terms of forces and moments resultants.

$$\delta u:\ N_{xx,x} = I_1\ddot{u} + I_2\ddot{\theta} \tag{42a}$$

$$\theta: M_{xx,x} - N_{xz} = I_2\ddot{u} + I_3\ddot{\theta} \tag{42b}$$

$$\delta w:\ N_{xz,x} - (N^T + N^E + N^M) w_{,xx} - K_1 w + K_2 w_{,xx} = I_1\ddot{w} \tag{42c}$$

$$\delta\psi: C_{x,x} + C_z = 0 \tag{42d}$$

$$\delta\varphi:\ F_{x,x} + F_z = 0 \tag{42e}$$

To obtain explicit governing equations, Eqs. (15), (16) and (19) are substituted into Eqs. (25), then combined with Eqs. (28)-(31). After all, they are integrated into Eq. (42) to result in the following governing equations.

$$I_1(\ddot{u} - \epsilon\ddot{u}_{,xx}) + I_2(\ddot{\theta} - \epsilon\ddot{\theta}_{,xx}) - A_{11}(u_{,xx} - \varrho u_{,xxxx}) - B_{11}(\theta_{,xx} - \varrho\theta_{,xxxx}) - G_e(\psi_{,x} - \varrho\psi_{,xxx}) - G_m(\varphi_{,x} - \varrho\varphi_{,xxx}) = 0 \tag{43a}$$

$$I_1(\ddot{w}-\epsilon\ddot{w}_{,xx})+(N^T+N^E+N^M)(w_{,xx}-\epsilon w_{,xxxx})+K_1(w-\epsilon w_{,xx})-K_2(w_{,xx}-\epsilon w_{,xxxx})-A_{22}(\theta_{,x}-\varrho\theta_{,xxx})-A_{22}(w_{,xx}-\varrho w_{,xxxx})+O_e(\psi_{,xx}-\varrho\psi_{,xxxx})+O_m(\varphi_{,xx}-\varrho\varphi_{,xxxx})=0 \quad (43b)$$

$$I_2(\ddot{u}-\epsilon\ddot{u}_{,xx})+I_3(\ddot{\theta}-\epsilon\ddot{\theta}_{,xx})-B_{11}(u_{,xx}-\varrho u_{,xxxx})-(A_{22}-P_{11})(\theta_{,xx}-\varrho\theta_{,xxxx})+A_{22}(w_{,x}-\varrho w_{,xxx})-(O_e+S_e)(\psi_{,x}-\varrho\psi_{,xxx})-(O_m+S_m)(\varphi_{,x}-\varrho\varphi_{,xxx})=0 \quad (43c)$$

$$T_z(u_{,x}-\varrho u_{,xxx})+(O_e+\bar{T}_z)(\theta_{,x}-\varrho\theta_{,xxx})+O_e(w_{,xx}-\varrho w_{,xxxx})+X_m(\psi_{,xx}-\varrho\psi_{,xxxx})-Y_m(\psi-\varrho\psi_{,xx})+X_e(\varphi_{,xx}-\varrho\varphi_{,xxx})-Y_e(\varphi-\varrho\varphi_{,xx})=0 \quad (43d)$$

$$R_z(u_{,x}-\varrho u_{,xxx})+(O_m+\bar{R}_z)(\theta_{,x}-\varrho\theta_{,xxx})+O_m(w_{,xx}-\varrho w_{,xxxx})+X_e(\psi_{,xx}-\varrho\psi_{,xxxx})-Y_e(\psi-\varrho\psi_{,xx})+\bar{X}_m(\varphi_{,xx}-\varrho\varphi_{,xxxx})-\bar{Y}_m(\varphi-\varrho\varphi_{,xx})=0 \quad (43e)$$

All coefficient A_{11}, B_{11}, A_{22}, P_{11}, G_e, G_m, O_e, O_m, S_e, S_m, T_z, $\bar{T}_z$, R_z, $\bar{R}_z$, X_e, X_m, $\bar{X}_e$, $\bar{X}_m$, Y_e, Y_m, $\bar{Y}_e$, $\bar{Y}_m$ are expressed in Appendix A.

3. Free vibration analysis

3.1 Solution procedure

Since the governing equations of motion (defined as Eq. (43)) are in form of coupled system of partial differential equations, Navier's method is conducted to discretize them. It is a popular analytical method that assumes the response to be trigonometric that is usually used for simple boundary conditions.

According to boundary conditions associated with the simply supported sandwich microbeam and using the procedure of References (Ansari *et al.* 2015, Karrubi *et al.* 2019), the Navier's type solution can be suggested as following series.

$$u(x,t)=\sum u_n\, cos(\zeta_n x)e^{i\omega t} \quad (44a)$$

$$w(x,t)=\sum w_n\, sin(\zeta_n x)\, e^{i\omega t} \quad (44b)$$

$$\theta(x,t)=\sum \theta_n\, cos(\zeta_n x)e^{i\omega t} \quad (44c)$$

$$\psi(x,t)=\sum \psi_n\, sin(\zeta_n x)e^{i\omega t} \quad (44d)$$

$$\varphi(x,t)=\sum \varphi_n\, sin(\zeta_n x)e^{i\omega t} \quad (44e)$$

in which $\zeta_n=n\pi/L$ and n denote mode number. Substituting the Navier's solution as in Eq. (44) into Eq. (43) yields ODEs as discretized governing equations of the sandwich microbeam

$$[M]\{\ddot{\chi}\}+[K]\{\chi\}=0 \quad (45a)$$

$$\{\chi\}=\{u_n\,, w_n\,, \theta_n\,, \psi_n\,, \varphi_n\}^T,\ \{\ddot{\chi}\}=-\omega^2\{\chi\} \quad (45b)$$

$$[M]=\begin{bmatrix} I_1(1+\epsilon{\zeta_n}^2) & 0 & I_2(1+\epsilon{\zeta_n}^2) & 0 & 0\\ 0 & I_1(1+\epsilon{\zeta_n}^2) & 0 & 0 & 0\\ I_2(1+\epsilon{\zeta_n}^2) & 0 & I_3(1+\epsilon{\zeta_n}^2) & 0 & 0\\ 0 & 0 & 0 & 0 & 0\\ 0 & 0 & 0 & 0 & 0 \end{bmatrix} \quad (45c)$$

$$[K]=\begin{bmatrix} K_{11} & K_{12} & K_{13} & K_{14} & K_{15}\\ K_{21} & K_{22} & K_{23} & K_{24} & K_{25}\\ K_{31} & K_{32} & K_{33} & K_{34} & K_{35}\\ K_{41} & K_{42} & K_{43} & K_{44} & K_{45}\\ K_{51} & K_{51} & K_{53} & K_{54} & K_{55} \end{bmatrix} \quad (45d)$$

where, K_{ij} arrays are defined in Appendix B.

The equations in the 4th and 5th rows can be solved in terms of displacement unknowns as follows

$$\varphi_n=a_1u_n+a_2w_n+a_3\theta_n \quad (46a)$$

$$\psi_n=a_4u_n+a_5w_n+a_6\theta_n \quad (46b)$$

Coefficients a_i in Eq. (46) are described in Appendix C.

Replacing Eq. (46) into Eq. (45) yields the following equations describing free vibration of the sandwich microbeam.

$$[M']\{\ddot{\chi}\}+[K']\{\chi\}=0 \quad (47a)$$

$$[M']=\begin{bmatrix} I_1(1+\epsilon{\zeta_n}^2) & 0 & I_2(1+\epsilon{\zeta_n}^2)\\ 0 & I_1(1+\epsilon{\zeta_n}^2) & 0\\ I_2(1+\epsilon{\zeta_n}^2) & 0 & I_3(1+\epsilon{\zeta_n}^2) \end{bmatrix} \quad (47b)$$

$$[K']=\begin{bmatrix} b_{11} & b_{12} & b_{13}\\ b_{21} & b_{22} & b_{23}\\ b_{31} & b_{32} & b_{33} \end{bmatrix} \quad (47c)$$

$$b_{11}=K_{11}+K_{14}a_4+K_{15}a_1 \quad (48a)$$

$$b_{12}=K_{12}+K_{14}a_5+K_{15}a_2 \quad (48b)$$

$$b_{13}=K_{13}+K_{14}a_6+K_{15}a_3 \quad (48c)$$

$$b_{21}=K_{21}+K_{24}a_5+K_{25}a_1 \quad (48d)$$

$$b_{22}=K_{22}+K_{24}a_5+K_{25}a_2 \quad (48e)$$

$$b_{23}=K_{23}+K_{24}a_6+K_{25}a_3 \quad (48f)$$

$$b_{31}=K_{31}+K_{34}\,a_4+K_{35}a_1 \quad (48g)$$

$$b_{32}=K_{32}+K_{34}a_5+K_{35}a_2 \quad (48h)$$

$$b_{33}=K_{33}+K_{34}a_6+K_{35}a_3 \quad (48i)$$

Note that by evaluating b_{ij} arrays as in Eq. (48), it will be realized that $[K']$ is a symmetric matrix.

Eventually, the natural frequencies of the sandwich microbeam can be obtained by inserting matrices $[M']$ and $[K']$ defined in Eq. (47) into the following equations.

Table 5 Geometry and material property parameters of the core for the verification study

$E_{core}\ (GPa)$	ν_{core}	$\rho_{core}\ (10^3\ kg/m^3)$
390	0.24	3.96
$L\ (nm)$	$b\ (nm)$	
10,000	1,000	

$$\Delta = [M']^{-1}[K'] \tag{49a}$$

$$\omega_n = \sqrt{eigenvalues(\Delta)} \tag{49b}$$

in which Δ and ω_n indicate dynamic matrix and the nth natural frequency of the sandwich microbeam, respectively.

The following free vibration analysis is presented based on the formulation of Eqs. (1)-(49). Also, to consider the effect of temperature-dependent properties, an additional diagram will be illustrated. It is estimated according to the following functions for E_M , α_M and $E_c^{\,0}$ (Mohammadimehr and Mostafavifar 2016).

$$E_M = 3.52 - 0.0034\Delta T\ (GPa) \tag{50a}$$

$$\alpha_M = 45(1 + 0.0005\Delta T) \times 10^{-6}\ (K^{-1}) \tag{50b}$$

$$\begin{gathered} E_c^{\,0} = -0.2398668972 \times 10^{-10}\Delta T^8 \\ +0.8099071975 \times 10^{-8}\Delta T^7 + 2.610124694\Delta T \\ -0.1126364748 \times 10^{-5}\Delta T^6 - \\ 0.8110540539\Delta T^2 + 0.00008247684020\Delta T^5 + \\ 0.07399495300\Delta T^3 - 0.003359420587\Delta T^4 + \\ 101.1755000\ (MPa) \end{gathered} \tag{50c}$$

3.2 Verification

As there are no available papers in the literature that consider all assumptions taken in this research simultaneously, an example which has investigated free vibration analysis of a Timoshenko microbeam via nonlocal theory is selected for a comparison study to check validity and accuracy of the present work.

Although the microbeam studied in Rahmani *et al.* (2014) is a single layer beam without any thermo-magneto-electric loads and porosity, it is the most consistent paper with the current one in mutual basic assumptions.

Owing to aforementioned differences between the two papers, the following assumptions are taken so that they become comparable.

- Thickness of GPL reinforced covers as well as piezo-magneto-electric face sheets are supposed approximately zero i.e., $h_g = h_p = 10^{-4}h_c$.
- Temperature change ΔT is equated to 10^{-4} (K) as if it is negligible.
- Coefficients of the Pasternak's foundation are assumed as $K_1 = 10^{-3}\ (N/m)$, $K_2 = 10^{-3}(Nm)$.
- Porosity coefficient e_0 is set 10^{-9}.
- Strain gradient parameter *l* is assumed zero in order to model nonlocal theory (neglecting strain gradient).

Other parameters are considered as listed in Table 5.

The fundamental natural frequency in Rahmani *et al.* (2014) is formulated in the following dimensionless form

$$\varpi_1 = \omega_1 L^2\sqrt{\rho_{core}A/E_{core}I} \tag{51}$$

in which, ω_1 indicates fundamental frequency expressed as in Eq. (49), A and I are area of beam's cross section and second inertia of its area, respectively ($A = bh, I = bh^3/12$).

Table 6 Comparison of dimensionless fundamental natural frequency

L/h_c	$\epsilon = e_0a = (\mu m^2)$	Rahmani *et al.* (2014)	Present	% Diff
20	0	9.830	10.124	2.991
	1	9.378	9.658	2.991
	2	8.983	9.252	2.992
	3	8.634	8.892	2.992
	4	8.323	8.572	2.992
	5	8.043	8.284	2.992
50	0	9.863	10.159	3.002
	1	9.410	9.692	3.002
	2	9.014	9.284	3.001
	3	8.664	8.924	3.002
	4	8.352	8.602	3.001
	5	8.071	8.313	3.001
100	0	9.868	10.162	2.984
	1	9.414	9.695	2.984
	2	9.018	9.287	2.984
	3	8.668	8.926	2.984
	4	8.356	8.605	2.984
	5	8.075	8.316	2.984

% Diff = 100 (value of present work – value of Ref.) / (value of Ref.)

Using Eq. (49) and taking into account the above assumptions, first dimensionless natural frequency can be validated as reported in Table 6 for various slenderness ratios in terms of nonlocal parameter. As it can be observed, the results of the present work are in good agreement with those of Rahmani *et al.* (2014) with a maximum difference of approximately 3 percent which is quite negligible since GPL covers, piezo-magneto-electric face sheets and Pasternak's foundation are not entirely removed, also thermal and porosity coefficients are not set exactly zero, but approximations are considered.

3.3 Numerical results

Hereafter, the numerical vibration analysis of thermal Timoshenko sandwich microbeam consisted of transversely flexible porous foam core and graphene reinforced nano-composite covers and piezo-magneto-electric face sheets resting on Pasternak's foundation is presented. The influence of various parameters of the system including geometry parameters in form of non-dimensional ratios, nonlocal strain gradient theory, distribution patters of GPL nanofillers as well as porosity, volume fraction of graphene nanofillers, porosity coefficient, elastic foundation,

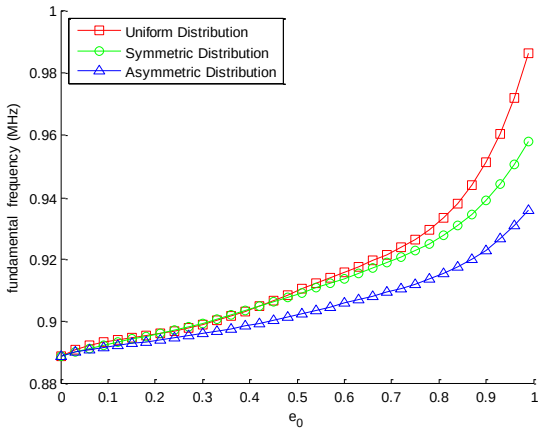

Fig. 4 Fundamental natural frequency vs. porosity coefficient for uniform, symmetric, asymmetric distribution patterns

temperature change and also different mode numbers which are illustrated one by one, either individually or simultaneously by means of tables or figures. The input data are considered as $L = 10\,\mu m, b = 10\,nm, L/h_c = 50,\ h_p/h_c = 0.1, h_p/h_g = 1/3\,, e_0 a/h_p = 1/10\,, l/e_0 a = 1,\ K_1 = 200(N/m), K_2 = 20(Nm),\ \Delta T = 10(℃), e_0 = 0.5,\ w^0_{GPL} = 1\%, n = 1$ and distribution patterns for porosity and GPLs are both uniform.

In Fig. 4, the effect of porosity distribution of the core on the fundamental natural frequency is investigated. For this purpose, three types of various distributions are considered i.e., uniform, symmetric and asymmetric. Also, e_0 is the porosity coefficient that varies between 0 and 0.9. By increasing e_0, the natural frequency for all three distributions increases because porous coefficient can decrease the mass density as well as the beam's structural stiffness, while the reduction for the mass density is higher than the stiffness of micro beam. It is seen from this figure that the uniform pattern gives the maximum changes; while for asymmetric distribution it is minimum. Also, for high porosity coefficients, the type of distribution is more important. The percentage of natural frequency increase for uniform distribution is 11.650%, for symmetric 8.137% and for asymmetric 5.552%.

The effect of different weight percentages with respect to ratio of h_g/h_c is investigated in Figs. 5(a)-(c) for uniform, linear and parabolic GPL distribution patterns, respectively. The natural frequency increases with increasing the thickness ratio since increasing thickness of graphene layer reinforces and consequently stiffens the structure. For the same reason, natural frequency increases with rising of GPL's weight percentage. On the other hands, increasing weight percentage of GPL leads to increase the stiffness of microbeam and then the natural frequency enhances. At low amounts of thickness ratio, the frequencies remain almost constant. Moreover, in all cases of distribution pattern, the largest frequency is gained when the weight percentage is 1% and the smallest is gained when it is 0%, because they mean highest and lowest reinforcement, respectively. It is seen that comparing the three figures demonstrates that the effect of weight

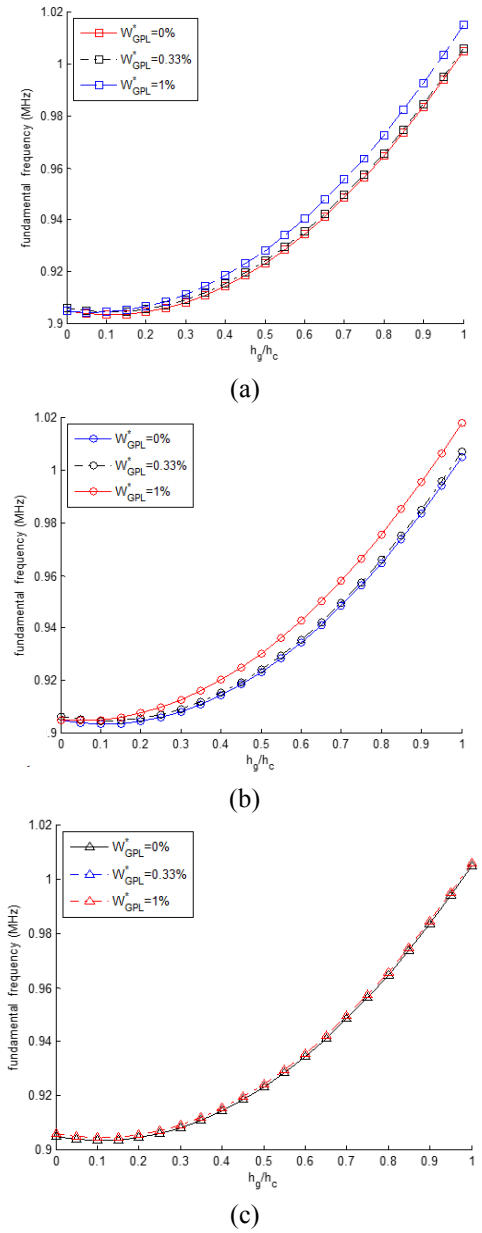

Fig. 5 Fundamental frequency vs. h_g/h_p for various weigh percentages, in case of (a) uniform GPL distribution; (b) linear GPL distribution; (c) parabolic GPL distribution

percentage in parabolic pattern is not as notable as in the other ones.

Table 7 deals with the effect of geometric ratios on the natural frequency. As shown, natural frequency decreases with an increase in L/h_c ratio because a longer beam acts more flexibly. However, increase in h_p/h_c ratio cause the growth of the natural frequency. Furthermore, $h_p/h_g = 1/3$ gives the highest natural frequency, which means that a greater thickness of the graphene reinforced layers yields higher natural frequency. The reason is the fact that thicker graphene platelets reinforced layer leads to better reinforcement and thus a stiffer structure.

In Table 8, the effect of GPL and porosity coefficient is investigated simultaneously. As the porosity coefficient grows, the natural frequency increases. It is expected that

Table 7 Fundamental natural frequency (MHz) vs. L/h_c for various thickness ratios (i.e., h_p/h_c and h_p/h_g)

L/h_c	h_p/h_g=0.5				h_p/h_g=1				h_p/h_g=3			
	h_p/h_c=0.1	h_p/h_c=0.5	h_p/h_c=1	h_p/h_c=3	h_p/h_c=0.1	h_p/h_c=0.5	h_p/h_c=1	h_p/h_c=3	h_p/h_c=0.1	h_p/h_c=0.5	h_p/h_c=1	h_p/h_c=3
10	44.200	81.501	94.563	115.610	39.736	70.265	89.875	112.005	37.816	60.660	78.879	109.698
20	25.213	57.779	78.858	98.961	22.323	42.452	61.890	98.082	21.245	34.441	48.666	85.725
30	18.441	43.069	64.781	93.905	16.887	29.853	45.515	84.169	16.393	23.919	34.336	67.567
40	15.612	33.975	53.917	88.177	15.015	23.108	35.628	72.298	14.918	18.588	26.448	54.819
50	14.476	28.020	45.744	82.305	14.569	19.065	29.210	62.677	14.741	15.544	21.582	45.760

Table 8 Fundamental natural frequency (MHz) vs. h_g/h_c for GPL percentile contents and porosity coefficients

h_g/h_c	W^0_{GPL}=0%			W^0_{GPL}=0.33%			W^0_{GPL}=1%		
	e_0=0.1	e_0=0.5	e_0=0.8	e_0=0.1	e_0=0.5	e_0=0.8	e_0=0.1	e_0=0.5	e_0=0.8
0.2	14.119	14.425	14.830	14.122	14.429	14.834	14.151	14.458	14.864
0.4	14.265	14.516	14.842	14.273	14.523	14.850	14.334	14.585	14.913
0.6	14.665	14.881	15.160	14.676	14.892	15.171	14.766	14.984	15.265
0.8	15.200	15.393	15.640	15.215	15.407	15.655	15.330	15.525	15.774
1.0	15.808	15.983	16.207	15.825	16.000	16.225	15.963	16.140	16.367

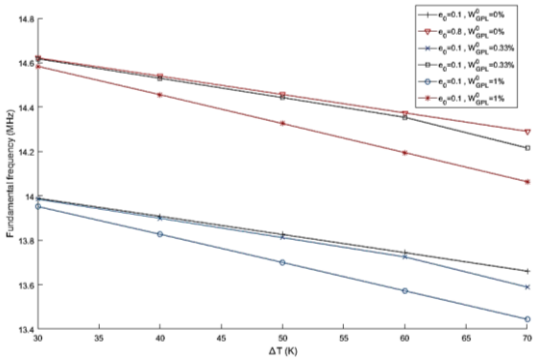

Fig. 6 Fundamental frequency vs. temperature change for various GPL percentile contents and porosity coefficients

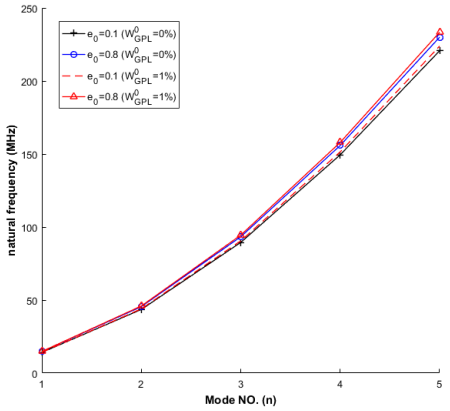

Fig. 7 Natural frequencies (MHz) for various GPL percentile contents and porosity coefficients

Table 9 Fundamental natural frequency (MHz) vs. Winkler coefficients for various shear layer coefficients

K_1	K_2=10	K_2=100	K_2=500
0	12.426	25.510	53.449
10^1	12.426	25.510	53.449
10^2	12.426	25.510	53.449
10^3	12.426	25.510	53.449
10^6	12.426	25.510	53.449
10^9	12.426	25.510	53.449
10^{12}	14.501	26.583	53.969
10^{13}	26.706	34.778	58.443
10^{14}	75.778	78.985	91.895
10^{15}	195.973	195.972	195.973

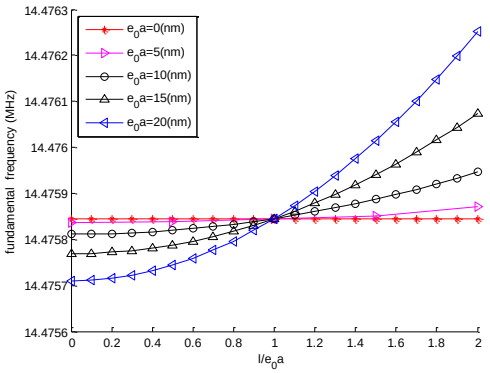

Fig. 8 Fundamental natural frequency vs. the material length scale to nonlocal parameters ratio for various values of nonlocal parameters

the natural frequency increases with increasing of weight percentage of graphene platelets as the structure is strengthened.

Fig. 6 shows that when the temperature of the structure increases, the natural frequency decreases for the fact that it is expected to expand and become softer, meaning more flexible. It can also be concluded that in case of higher GPL weight percentage, the temperature change has a sharper effect on the natural frequency. But it does not matter significantly for the porosity coefficient.

In Fig. 7, the effect of mode number is investigated. It is

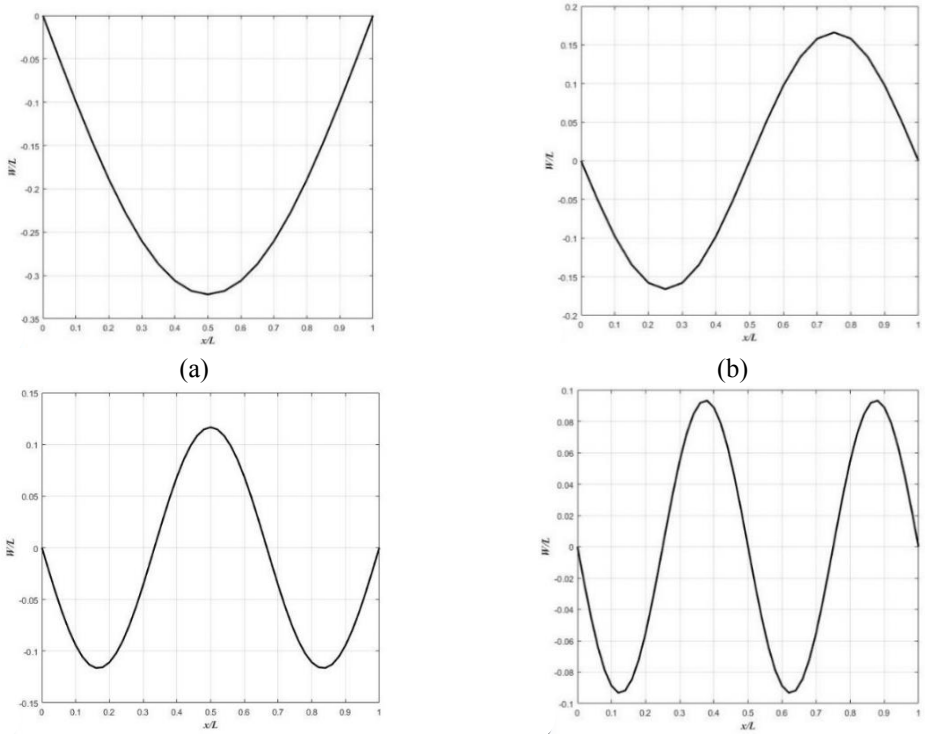

(a) (b)

(c) (d)

Fig. 9 Mode shape of the microbeam for (a) n=1; (b) n=2; (c) n=3; (d) n=4

overall seen that the structure has a higher natural frequency at higher modes such that the 5th mode is about 5 times more that the 1st mode. Also, it clarifies that at any mode, the natural frequency increases with an increase in GPL's weight percentage or decrease in porosity coefficients, which were previously proved in detail for the fundamental natural frequency (i.e., the first mode).

Table 9 examines the effect of the Pasternak elastic coefficients in a large range. K_1 is the Winkler coefficient and K_2 is the shear layer coefficient. By increasing K_1 from 0 to 10^9, this coefficient has no remarkable effect on the natural frequency, because in the governing equations which carry K_1, its corresponding terms are negligible compared to the other terms except in very large values. But after the value of $K_1$is more 10^9, it begins to increase the natural frequency. Also, it is concluded that with an increase in K_2, the natural frequency increases. It seems that variation of shear layer coefficient can cause more changes in comparison with the Winkler coefficient. On the other hands, they both make the structure stiffer and hence generate a higher natural frequency.

Fig. 8 shows the effect of nonlocal parameter e_0a and strain gradient parameter l in a dimensionless form. As l/e_0a increases, the natural frequency rises. That happens since increase in l/e_0a means increase in l or decrease in e_0a; the first one implies more stiff-hardening and the second one implies less stiff-softening; so they both result in growth of natural frequency. It is noted that e_0a/l=1 means $=\varrho$, so the terms $(1-\epsilon\nabla^2)$ and $(1-\varrho\nabla^2)$ are simplified from constitutive equations. As a result, value of e_0a does not change frequency.

Fig. 9 shows the mode shape of the microbeam along its length for n=1, 2, 3, 4. It is obvious that with each increase in the mode number (n), the number of peaks and nodes increases of one.

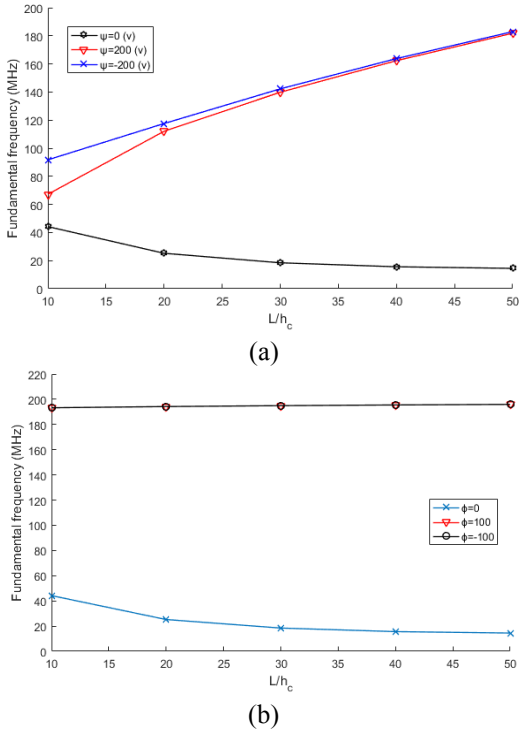

(a)

(b)

Fig. 10 Fundamental natural frequency vs. L/h_c for various values of (a) ψ_0; (b) ϕ_0

Fig. 10 shows the effect of applied electric potential (Fig. 10(a)) and magnetic potential (Fig. 10(b)) in terms of

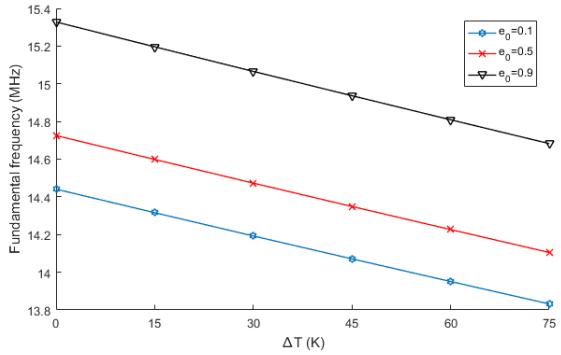

Fig. 11 Fundamental natural frequency vs. ΔT for various values of porosity coefficient based on Eq. (50)

L/h_c ratio. As it shows, when $\psi_0 = 0$, the natural frequency increases with L/h_c, but when $\psi_0 = 200, -200$, it decreases. Moreover, when $\phi_0 = 0$, natural frequency increases with L/h_c, but it is the reverse when $\phi_0 = 100, -100$. It is seen that with considering ψ_0 and ϕ_0, the microbeam becomes softer, thus the natural frequency decreases.

As the mentioned before, the effect of temperature change on natural frequency is analyzed assuming that the materials are temperature dependent based on Eq. (50). Fig. 11 demonstrates for various porosity coefficients based on temperature-dependent properties. It is seen that fundamental frequency decreases with temperature change for all of the porosity coefficients. On the other hands, with increasing of temperature change, the stiffness of microbeam decreases.

4. Conclusions

In this research, five layers Timoshenko microbeam including a transversely flexible porous foam core covered by GPL nanocomposite reinforced sheets and piezo-magneto-electric face sheets in uniform thermal environment resting on a Pasternak foundation is investigated. The linear constitutive equations are employed based on nonlocal strain gradient theory. Also, the Hamilton's principle is used to derive the governing equations which are then solved by Navier's technique. The discovered results dealing with frequency analysis can be summarized as the following headlines which can hopefully aid specialists for the future nanotechnology explorations and inventions, especially for resonance characterizations that demonstrates the application of this paper.

- Among the three proposed patterns for porosity throughout the thickness of the core, uniform and asymmetric patterns result in highest and lowest natural frequencies, respectively. Also, it is demonstrated the highest and lowest sensitivity towards value of porosity, respectively.
- Comparing the effects of three patterns suggested for distribution of GPL nanofillers through the thickness of GPL reinforced covers, linear pattern offers safer structure, especially when mixing more graphene nanofillers; on the other hand, uniform pattern is the least helpful one.
- It is demonstrated the highest and lowest sensitivity towards value of porosity, respectively.
- Although increasing the thickness of any layer makes the structure heavier, thicker GPL layer can intensify the natural frequency because of enhancing the stiffness.
- Designers may be able to perform a safer construction by considering a thinner foam core compared to other layers.
- Thickness of piezo-magneto-electric face sheets is moderately more effective than that of the core, while it is totally the reverse in comparison with that of GPL covers.
- A slenderer microbeam serves a more probable resonance as it approaches a wire.
- The microbeam acts more flexible in higher temperatures which means less natural frequency is gained. Generally, the role of temperature might be bolder by having less porosity but more graphene nanofillers. It is worth mentioning that all of natural frequencies (i.e., corresponding with any mode number) follow the same trend.
- It can be generally claimed that raising the both coefficients of Pasternak foundation (i.e., shear layer and Winkler springs) yields higher natural frequencies because the microstructure becomes stiffer, but the influence of shear layer is more significant than Winkler foundation. Getting deeper into the results will prove the fact that as the intensity of one of these two parameters increases, the sensitivity of natural frequency to the other one decreases.
- It is seen that with considering ψ_0 and ϕ_0, the microbeam becomes softer, thus the natural frequency decreases.

It is seen that fundamental frequency decreases with temperature change for all the porosity coefficients. On the other hands, with increasing of temperature change, the stiffness of microbeam decreases.

Acknowledgements

The authors would like to thank the referees for their valuable comments. Also, they are thankful to the Iranian Nanotechnology Development Committee for supporting this research and the University of Kashan under Grant No. 8911238/14.

References

Addou, F.Y., Meradjah, M., Bousahla, A.A., Benachour, A., Bourada, F., Tounsi, A. and Mahmoud, S.R. (2019), "Influences of porosity on dynamic response of FG plates resting on Winkler/Pasternak/Kerr foundation using quasi 3D HSDT", *Comput. Concrete*, **24**(4), 347-367. https://doi.org/10.12989/cac.2019.24.4.347.

Adeniyi, A.G., Adeoye, S.A., Onifade, D.V. and Joshua, O.I. (2019), "Multi-scale finite element analysis of effective elastic property of sisal fiber-reinforced polystyrene composites", *Mech. Adv. Mater. Struct.*, 1-9.

https://doi.org/10.1080/15376494.2019.1660016.

Akgöz, B. and Civalek, Ö. (2018), "Vibrational characteristics of embedded microbeams lying on a two-parameter elastic foundation in thermal environment", *Compos. B. Eng*., **150**, 68-77. https://doi.org/10.1016/j.compositesb.2018.05.049.

AkhavanAlavi, S.M., Mohammadimehr, M. and Edjtahed, S.H. (2019), "Active control of micro Reddy beam integrated with functionally graded nanocomposite sensor and actuator based on linear quadratic regulator method", *Eur. J. Mech. A-Solid*, **74**, 449-461. https://doi.org/10.1016/j.euromechsol.2018.12.008.

Amir, S., Bidgoli, E.M.R. and Arshid, E. (2018), "Size-dependent vibration analysis of a three-layered porous rectangular nano plate with piezo-electromagnetic face sheets subjected to pre loads based on SSDT", *Mech. Adv. Mater. Struct.*, 1-15. https://doi.org/10.1080/15376494.2018.1487612.

Anitescu, C., Atroshchenko, E., Alajlan, N. and Rabczuk, T. (2019), "Artificial neural network methods for the solution of second order boundary value problems", *Comput. Mater. Contin.*, **59**(1), 345-359. https:// doi:10.32604/cmc.2019.06641.

Ansari, R., Gholami, R. and Rouhi, H. (2015), "Size-dependent nonlinear forced vibration analysis of magneto-electro-thermo-elastic Timoshenko nanobeams based upon the nonlocal elasticity theory", *Compos. Struct.*, **126**, 216-226. https://doi.org/10.1016/j.compstruct.2015.02.068.

Apuzzo, A., Barretta, R., Faghidian, S.A., Luciano, R. and Marotti de Sciarra, F. (2018), "Free vibrations of elastic beams by modified nonlocal strain gradient theory", *Int. J. Eng. Sci.*, **133**, 99-108. https://doi.org/10.1016/j.ijengsci.2018.09.002.

Arefi, M., Bidgoli, E.M.R., Dimitri, R. and Tornabene, F. (2018a), "Free vibrations of functionally graded polymer composite nanoplates reinforced with graphene nanoplatelets", *Aerosp. Sci. Technol.*, **81**, 108-117. https://doi.org/10.1016/j.ast.2018.07.036.

Arefi, M., Karroubi, R. and Irani-Rahaghi, M. (2016), "Free vibration analysis of functionally graded laminated sandwich cylindrical shells integrated with piezoelectric layer", *Appl. Math. Mech.*, **37**(7), 821-834. https://doi.org/10.1007/s10483-016-2098-9.

Arefi, M., Kiani, M. and Rabczuk, T. (2019), "Application of nonlocal strain gradient theory to size dependent bending analysis of a sandwich porous nanoplate integrated with piezomagnetic face-sheets", *Compos. B. Eng.*, **168**, 320-333. https://doi.org/10.1016/j.compositesb.2019.02.057.

Arefi, M., Zamani, M.H. and Kiani, M. (2018b), "Size-dependent free vibration analysis of three-layered exponentially graded nanoplate with piezomagnetic face-sheets resting on Pasternak's foundation", *J. Int. Mater. Syst. Struct.*, **29**(5), 774-786. https://doi.org/10.1177/1045389X17721039.

Balubaid, M., Tounsi, A., Dakhel, B. and Mahmoud, S.R. (2019), "Free vibration investigation of FG nanoscale plate using nonlocal two variables integral refined plate theory", *Comput. Concrete*, **24**(6), 579-586. https://doi.org/10.12989/cac.2019.24.6.579.

Bamdad, M., Mohammadimehr, M. and Alambeigi, K. (2019), "Analysis of sandwich Timoshenko porous beam with temperature-dependent material properties: Magneto-electro-elastic vibration and buckling solution", *J. Vib. Control*, **25**(23-24), 2875-2893. https://doi.org/10.1177/1077546319860314.

Barati, M.R. and Zenkour, A.M. (2017), "Post-buckling analysis of refined shear deformable graphene platelet reinforced beams with porosities and geometrical imperfection", *Compos. Struct.*, **181**, 194-202. https://doi.org/10.1016/j.compstruct.2017.08.08.2

Baroudi, S. and Najar, F. (2019), "Dynamic analysis of a nonlinear nanobeam with flexoelectric actuation", *J. Appl. Phys.*, **125**(4), 044503. https://doi.org/10.1063/1.5057727.

Bedia, W.A., Houari, M.S.A., Bessaim, A., Bousahla, A.A., Tounsi, A., Saeed, T. and Alhodaly, M.S. (2019), "A new hyperbolic two-unknown beam model for bending and buckling analysis of a nonlocal strain gradient nanobeams", *J. Nano Res.*, **57**, 175-191. https://doi.org/10.4028/www.scientific.net/JNanoR.57.175.

Berghouti, H., Adda Bedia, E.A., Benkhedda, A. and Tounsi, A. (2019), "Vibration analysis of nonlocal porous nanobeams made of functionally graded material", *Adv. Nano Res.*, **7**(5), 351-364. https://doi.org/10.12989/anr.2019.7.5.351.

Boukhlif, Z., Bouremana, M., Bourada, F., Bousahla, A.A., Bourada, M., Tounsi, A. and Al-Osta, M.A. (2019), "A simple quasi-3D HSDT for the dynamics analysis of FG thick plate on elastic foundation", *Steel Compos. Struct.*, **31**(5), 503-516. https://doi.org/10.12989/scs.2019.31.5.503.

Boulefrakh, L., Hebali, H., Chikh, A., Bousahla, A.A., Tounsi, A. and Mahmoud, S.R. (2019), "The effect of parameters of visco-Pasternak foundation on the bending and vibration properties of a thick FG plate", *Geomech. Eng.*, **18**(2), 161-178. https://doi.org/10.12989/gae.2019.18.2.161.

Bourada, F., Bousahla, A.A., Bourada, M., Azzaz, A., Zinata, A. and Tounsi, A. (2019), "Dynamic investigation of porous functionally graded beam using a sinusoidal shear deformation theory", *Wind Struct.*, **28**(1), 19-30. https://doi.org/10.12989/was.2019.28.1.019.

Boutaleb, S., Benrahou, K.H., Bakora, A., Algarni, A., Bousahla, A.A., Tounsi, A., Tounsi, A. and Mahmoud, S.R. (2019), "Dynamic Analysis of nanosize FG rectangular plates based on simple nonlocal quasi 3D HSDT", *Adv. Nano Res.*, **7**(3), 189-206. https://doi.org/10.12989/anr.2019.7.3.191.

Bui, T.Q., Khosravifard, A., Zhang, Ch. Hematiyan, M.R. and Golub, M.V. (2013), "Dynamic analysis of sandwich beams with functionally graded core using a truly meshfree radial point interpolation method", *Eng. Struct.*, **47**, 90-104. https://doi.org/10.1016/j.engstruct.2012.03.041.

Chaabane, L.A., Bourada, F., Sekkal, M., Zerouati, S., Zaoui, F.Z., Tounsi, A., Derras, A., Bousahla, A.A. and Tounsi, A. (2019), "Analytical study of bending and free vibration responses of functionally graded beams resting on elastic foundation", *Struct. Eng. Mech.*, **71**(2), 185-196. https://doi.org/10.12989/sem.2019.71.2.185.

Chan, D.Q., Nguyen, P.D., Quang, V.D., Anh, V.T.T. and Duc, N.D. (2018), "Nonlinear buckling and post-buckling of functionally graded CNTs reinforced composite truncated conical shells subjected to axial load", *Steel Compos. Struct.*, **31**(3), 243-259. https://doi.org/10.12989/scs.2019.31.3.243.

Chen, D. Yang, J. and Kitipornchai, S. (2017), "Nonlinear vibration and postbuckling of functionally graded graphene reinforced porous nanocomposite beams", *Compos. Sci. Technol.*, **142**, 235-245. https://doi.org/10.1016/j.compscitech.2017.02.008.

Dong, Y., Li, X., Gao, K., Li, Y. and Yang, J. (2020b), "Harmonic resonances of graphene-reinforced nonlinear cylindrical shells: effects of spinning motion and thermal environment", *Nonlinear Dyn.*, **99**, 981-1000. https://doi.org/10.1007/s11071-019-05297-8.

Dong, Y., Li, Y., Li, X. and Yang, J. (2020a), "Active control of dynamic behaviors of graded graphene reinforced cylindrical shells with piezoelectric actuator/sensor layers", *App. Math. Model.*, **82**, 252-270. https://doi.org/10.1016/j.apm.2020.01.054.

Dong, Y.H., Li, Y.H., Chen, D. and Yang, J. (2018a), "Vibration characteristics of functionally graded graphene reinforced porous nanocomposite cylindrical shells with spinning motion", *Compos. B. Eng.*, **145**, 1-13. https://doi.org/10.1016/j.compositesb.2018.03.009.

Dong, Y.H., Zhu, B., Wang, Y., He, L.W., Li, Y.H. and Yang, J. (2019), "Analytical prediction of the impact response of graphene reinforced spinning cylindrical shells under axial and thermal loads", *Appl. Math. Model.*, **71**, 331-348. https://doi.org/10.1016/j.apm.2019.02.024.

Dong, Y.H., Zhu, B., Wang, Y., Li, Y.H. and Yang, J. (2018b), "Nonlinear free vibration of graded graphene reinforced cylindrical shells: Effects of spinning motion and axial load", *J. Sound Vib.*, **437**, 79-96. https://doi.org/10.1016/j.jsv.2018.08.036.

Draiche, K., Bousahla, A.A., Tounsi, A., Alwabli, A.S., Tounsi, A. and Mahmoud, S.R. (2019), "Static analysis of laminated reinforced composite plates using a simple first-order shear deformation theory", *Comput. Concrete*, **24**(4), 369-378. https://doi.org/10.12989/cac.2019.24.4.369.

Draoui, A., Zidour, M., Tounsi, A. and Adim, B. (2019), "Static and dynamic behavior of nanotubes-reinforced sandwich plates using (FSDT)", *J. Nano Res.*, **57**, 117-135. https://doi.org/10.4028/www.scientific.net/JNanoR.57.117.

Ebrahimi, F. and Barati, M.R. (2017), "Hygrothermal effects on vibration characteristics of viscoelastic FG nanobeams based on nonlocal strain gradient theory", *Compos. Struct.*, **159**, 433-444. https://doi.org/10.1016/j.compstruct.2016.09.092.

Ebrahimi, F. and Dabbagh, A. (2018), "Wave dispersion characteristics of embedded graphene platelets-reinforced composite microplates", *Eur. Phys. J. Plus*, **133**, 151. https://doi.org/10.1140/epjp/i2018-11956-5.

Ebrahimi, F. and Salari, E. (2015), "Thermo-mechanical vibration analysis of nonlocal temperature-dependent FG nanobeams with various boundary conditions", *Compos. B. Eng.*, **78**, 272-290. https://doi.org/10.1016/j.compositesb.2015.03.068.

Fang, W., Yu, T., Lich, L.V. and Bui, T.Q. (2019), "Analysis of thick porous beams by a quasi-3D theory and isogeometric analysis", *Compos. Struct.*, **221**, 110890. https://doi.org/10.1016/j.compstruct.2019.04.062.

Farajpour, M.R., Shahidi, A.R., Hadi, A. and Farajpour, A. (2019), "Influence of initial edge displacement on the nonlinear vibration, electrical and magnetic instabilities of magneto-electro-elastic nanofilms", *Mech. Adv. Mater. Struct.*, **26**(17), 1469-1481. https://doi.org/10.1080/15376494.2018.1432820.

Ganapathi, M., Anirudh, B., Anant, C. and Polit, O. (2019), "Dynamic characteristics of functionally graded graphene reinforced porous nanocomposite curved beams based on trigonometric shear deformation theory with thickness stretch effect", *Mech Adv. Mater. Struct.*, 1-12. https://doi.org/10.1080/15376494.2019.1601310.

Ghasemi, H.S., Park, H. and Rabczuk, T. (2017), "A level-set based IGA formulation for topology optimization of flexoelectric materials", *Comput. Methods Appl. Mech. Eng.*, **313**, 239-258. https://doi.org/10.1016/j.cma.2016.09.029.

Ghasemi, H.S., Park, H. and Rabczuk, T. (2018), "A multi-material level set-based topology optimization of flexoelectric composites", *Comput. Methods Appl. Mech. Eng.*, **332**, 47-62. https://doi.org/10.1016/j.cma.2017.12.005.

Ghorbanpour Arani, A. and Zamani, M.H. (2018), "Nonlocal free vibration analysis of FG-porous shear and normal deformable sandwich nanoplate with piezoelectric face sheets resting on silica aerogel foundation", *Arab. J. Sci. Eng.*, **43**(9), 4675-4688. https://doi.org/10.1007/s13369-017-3035-8.

Ghorbanpour Arani, A. and Zamani, M.H. (2019), "Investigation of electric field effect on size-dependent bending analysis of functionally graded porous shear and normal deformable sandwich nanoplate on silica Aerogel foundation", *J. Sandw. Struct. Mater.*, **21**(8), 2700-2734. https://doi.org/10.1177/1099636217721405.

Ghorbanpour Arani, A. Babaakbar Zarei, H. and Pourmousa, P. (2019), "Free vibration response of FG porous sandwich micro-beam with flexoelectric face-sheets resting on modified Silica Aerogel foundation", *Int. J. Appl. Mech.*, **11**(09), 1950087. https://doi.org/10.1142/S175882511950087x.

Ghorbanpour Arani, A. Khani, M. and Khoddami Maraghi, Z. (2018), "Dynamic analysis of a rectangular porous plate resting on an elastic foundation using high-order shear deformation theory", *J. Vib. Control*, **24**(16), 3698-3713. https://doi.org/10.1177/1077546317709388.

Ghorbanpour Arani, A., Khoddami Maraghi, Z., Khani, M. and Alinaghian, I. (2017), "Free vibration of embedded porous plate using third-order shear deformation and poroelasticity theories", *J. Eng.*, **2017**, Article ID 1474916, 13. https://doi.org/10.1155/2017/1474916.

Ghorbanpour Arani, A., Rousta Navi, B. and Mohammadimehr, M. (2016), "Surface stress and agglomeration effects on nonlocal biaxial buckling polymeric nanocomposite plate reinforced by CNT using various approaches", *Adv. Compos. Mater.*, **25**(5), 423-441. https://doi.org/10.1080/09243046.2015.1052189.

Hajmohammad, M.H., Zarei, M.S., Sepehr, M. and Abtahi, N. (2018), "Bending and buckling analysis of functionally graded annular microplate integrated with piezoelectric layers based on layerwise theory using DQM", *Aerosp. Sci. Technol.*, **79**, 679-688. https://doi.org/10.1016/j.ast.2018.05.055.

Halpin, J.C. and Kardos, J.L. (1976), "The Halpin-Tsai equations: a review", *Polym. Eng. Sci.*, **16**(5), 344-352. https://doi.org/10.1002/pen.760160512.

Hamdia, M., Ghasemi, Kh., Zhuang, H., Alajlan, X.N. and Rabczuk, T. (2018), "Sensitivity and uncertainty analysis for flexoelectric nanostructures", *Comput. Meth. Appl. Mech. Eng.*, **337**, 95-109. https://doi.org/10.1016/j.cma.2018.03.016.

Heydari, A. (2018), "Exact vibration and buckling analyses of arbitrary gradation of nano-higher order rectangular beam", *Steel Compos Struct.*, **28**(5), 589-606. https://doi.org/10.12989/scs.2018.28.5.589.

Hussain, M., Nawaz Naeem, M., Tounsi, A. and Taj, M. (2019), "Nonlocal effect on the vibration of armchair and zigzag SWCNTs with bending rigidity", *Adv. Nano Res.*, **7**(6), 431-442. https://doi.org/10.12989/anr.2019.7.6.431.

Jandaghian, A. and Rahmani, O. (2016), "Free vibration analysis of magneto-electro-thermo-elastic nanobeams resting on a Pasternak foundation", *Smart Mater. Struct.*, **25**(3), 035023. https://doi.org/10.1088/0964-1726/25/3/035023.

Javani, R., Rabani Bidgoli, M. and Kolahchi, R. (2019), "Buckling analysis of plates reinforced by Graphene platelet based on Halpin-Tsai and Reddy theories", *Steel Compos. Struct., Int. J.*, **31**(4), 419-427. https://doi.org/10.12989/scs.2019.31.4.419.

Kaddari, M., Kaci, Bousahla, A.A., Tounsi, A. Bourada, F., Tounsi, A., Bedia, E.A.A. and Al-Osta, M.A. (2020), "A study on the structural behaviour of functionally graded porous plates on elastic foundation using a new quasi-3D model: Bending and Free vibration analysis", *Comput. Concrete*, **25**(1), 37-57. https://doi.org/10.12989/cac.2020.25.1.037.

Karami, B., Janghorban, M. and Tounsi, A. (2019), "Galerkin's approach for buckling analysis of functionally graded anisotropic nanoplates/different boundary conditions", *Eng. Comput.*, **35**, 1297-1316. https://doi.org/10.1007/s00366-018-0664-9.

Karami, B., Janghorban, M. and Tounsi, A. (2019), "Galerkin's approach for buckling analysis of functionally graded anisotropic nanoplates/different boundary conditions", *Eng. Comput.*, **35**, 1297-1316. https://doi.org/10.1007/s00366-018-0664-9.

Karimiasl, M., Kargarfard, K. and Ebrahimi, F. (2019), "Buckling of magneto-electro-hygro-thermal piezoelectric nanoplates system embedded in a visco-Pasternak medium based on nonlocal theory", *Microsyst. Techol.*, **25**(3), 1031-1042. https://doi.org/10.1007/s00542-018-4148.

Karroubi, R. and Irani-Rahaghi, M. (2019), "Rotating sandwich cylindrical shells with an FGM core and two FGPM layers: free vibration analysis", *Appl. Math. Mech.*, **40**(4), 563-578. https://doi.org/10.1016/j.compositesb.2013.03.008.

Khaniki, H.B. Hashemi, H. and Nezamabadi, A. (2018), "Buckling analysis of nonuniform nonlocal strain gradient beams using generalized differential quadrature method", *Alex. Eng. J.*, **57**(3), 1361-1368. https://doi.org/10.1016/j.aej.2017.06.001.

Khiloun, M., Bousahla, A.A., Kaci, A., Bessaim, A., Tounsi. A. and Mahmoud, S.R. (2019), "Analytical modeling of bending and vibration of thick advanced composite plates using a four-variable quasi 3D HSDT", *Eng. Comput.*, **36**, 807-821. https://doi.org/10.1007/s00366-019-00732-1.

Kiani, Y. and Mirzaei, M. (2019), "Isogeometric thermal postbuckling of FG-GPLRC laminated plates", *Steel Compos. Struct*., **32**(6), 821-832. https://doi.org/10.12989/scs.2019.32.6.821.

Kim, C., Ko, Y., Kim, T., Yoo, C.S., Choi, B., Han, S.H. Jang, Y.H., Kim, Y. and Kim, N. (2018), "Design and evaluation of an experimental system for monitoring the mechanical response of piezoelectric energy harvesters", *Smart Struct. Syst*., **22**(2), 133-137. https://doi.org/10.12989/sss.2018.22.2.133.

Kitipornchai, S., Chen, D. and Yang, J. (2017), "Free vibration and elastic buckling of functionally graded porous beams reinforced by graphene platelets", *Mater. Des.*, **116**, 656-665. https://doi.org/10.1016/j.matdes.2016.12.061.

Kumar, B.R. and Hariharan, S.S. (2019), "Experimental and microstructural evaluation on mechanical properties of sisal fibre reinforced bio-composites", *Steel Compos. Struct.*, **33**(2), 299-306. https://doi.org/10.12989/scs.2019.33.2.299.

Li, L. and Hu, Y. (2016), "Nonlinear bending and free vibration analyses of nonlocal strain gradient beams made of functionally graded material", *Int. J. Eng. Sci.*, **107**, 77-97. https://doi.org/10.1016/j.ijengsci.2016.07.011.

Liu, C., Ke, L.L., Wang, Y.S., Yang, J. and Kitipornchai, S. (2013), "Thermo-electro-mechanical vibration of piezoelectric nanoplates based on the nonlocal theory", *Compos. Struct*., **106**, 167-174. https://doi.org/10.1016/j.compstruct.2013.05.031.

Liu, H., Lv, Z. and Wu, H. (2019a), "Nonlinear free vibration of geometrically imperfect functionally graded sandwich nanobeams based on nonlocal strain gradient theory", *Compos. Struct.*, **214**, 47-61. https://doi.org/10.1016/j.compstruct.2019.01.090.

Liu, S., Yu, T., van Lich, L., Yin, S. and Bui, Q.T. (2018), "Size effect on cracked functional composite microplates by an XIGA-based effective approach", *Meccanica*, **53**, 2637-2658. https://doi.org/10.1007/s11012-018-0848-9.

Liu, S., Yu, T., van Lich, L., Yin, S. and Bui, T.Q. (2019b), "Size and surface effects on mechanical behavior of thin nanoplates incorporating microstructures using isogeometric analysis", *Compos. Struct.*, **212**, 173-187. https://doi.org/10.1016/j.compstruc.2018.10.009.

Lu, L., Guo, X. and Zhao, J. (2017a), "Size-dependent vibration analysis of nanobeams based on the nonlocal strain gradient theory", *Int. J. Eng. Sci.*, **116**, 12-24. https://doi.org/10.1016/j.ijengsci.2017.03.006.

Lu, L., Guo, X. and Zhao, J. (2017b), "A unified nonlocal strain gradient model for nanobeams and the importance of higher order terms", *Int. J. Eng. Sci.*, **119**, 265-277. https://doi.org/10.1016/j.ijengsci.2017.06.024.

Mahesh, V., Kattimani, S., Harursampath, D. and Trung, N.T. (2019), "Coupled evaluation of the free vibration characteristics of magneto-electro-elastic skew plates in hygrothermal environment", *Smart Struct. Syst*., **24**(2), 267-292. https://doi.org/10.12989/sss.2019.24.2.267.

Mahmoudi, A., Benyoucef, S., Tounsi, A., Benachour, A., Adda Bedia, E.A. and Mahmoud, S.R. (2019), "A refined quasi-3D shear deformation theory for thermo-mechanical behavior of functionally graded sandwich plates on elastic foundations", *J. Sandw. Struct. Mater*., **21**(6), 1906-1926. https://doi.org/10.1177/1099636217727577.

Marzbanrad, J., Boreiry, M. and Shaghaghi, G.R. (2017), "Surface effects on vibration analysis of elastically restrained piezoelectric nanobeams subjected to magneto-thermo-electrical field embedded in elastic medium", *Appl. Phys. A*, **123**(4), 246. https://doi.org/10.1007/s00339-017-0768-x.

Medani, M., Benahmed, A., Zidour, M., Heireche, H., Tounsi, A., Bousahla, A.A., Tounsi, A. and Mahmoud, S.R. (2019), "Static and dynamic behavior of (FG-CNT) reinforced porous sandwich plate", *Steel Compos. Struct*., **32**(5), 595-610. https://doi.org/10.12989/scs.2019.32.5.595.

Mirjavadi, S., Afshari, B.M., Barati, M.R. and Hamouda, A.M.S. (2019), "Nonlinear free and forced vibrations of graphene nanoplatelet reinforced microbeams with geometrical imperfection", *Microsyst. Technol.*, **25**, 3137-3150. https://doi.org/10.1007/s00542-018-4277-4.

Mohammadimehr, M. and Alimirzaei, S. (2016), "Nonlinear static and vibration analysis of Euler-Bernoulli composite beam model reinforced by FG-SWCNT with initial geometrical imperfection using FEM", *Struct. Eng. Mech*., **59**(3), 431-454. https://doi.org/10.12989/sem.2016.59.3.431.

Mohammadimehr, M. and Mostafavifar, M. (2016), "Free vibration analysis of sandwich plate with a transversely flexible core and FG-CNTs reinforced nanocomposite face sheets subjected to magnetic field and temperature-dependent material properties using SGT", *Compos. B. Eng*., **94**, 253-270. https://doi.org/10.1016/j.compositesb.2016.03.030.

Mohammadimehr, M. and Shahedi, S. (2017), "High-order buckling and free vibration analysis of two types sandwich beam including AL or PVC-foam flexible core and CNTs reinforced nanocomposite face sheets using GDQM", *Compos. B. Eng.*, **108**, 91-107. https://doi.org/10.1016/j.compositesb.2016.09.040.

Mohammadimehr, M., Atifeh, S.J. and Navi, B.R. (2018), "Stress and free vibration analysis of piezoelectric hollow circular FG-SWBNNTs reinforced nanocomposite plate based on modified couple stress theory subjected to thermo-mechanical loadings", *J. Vib. Control*, **24**(15), 3471-3486. https://doi.org/10.1177/1077546317706887.

Mohammadimehr, M., Mohammadimehr, M.A. and Dashti, P. (2016), "Size-dependent effect on biaxial and shear nonlinear buckling analysis of nonlocal isotropic and orthotropic micro-plate based on surface stress and modified couple stress theories using differential quadrature method", *Appl. Math. Mech.*, **37**(4), 529-554. https://doi.org/10.1007/s10483-016-2045-9.

Mohammadimehr, M., Navi, B.R. and Arani, A.R. (2017b), "Dynamic stability of modified strain gradient theory sinusoidal viscoelastic piezoelectric polymeric functionally graded single-walled carbon nanotubes reinforced nanocomposite plate considering surface stress and agglomeration effects under hydro-thermo-electro-magneto-mechanical loadings", *Mech. Adv. Mater. Struct.*, **24**(16), 1325-1342. https://doi.org/10.1080/15376494.2016.1227507.

Mohammadimehr, M., Saidi, A.R., Arani, A.G, Arefmanesh, A. and Han, Q. (2010), "Torsional buckling of a DWCNT embedded on Winkler and Pasternak foundations using nonlocal theory", *J. Mech. Sci. Technol.*, **24**(6), 1289-1299. ttps://doi.org/10.1007/s12206-010-0331-6.

Mohammadimehr, M., Shahedi, S. and Navi, B.R. (2017a), "Nonlinear vibration analysis of FG-CNTRC sandwich Timoshenko beam based on modified couple stress theory subjected to longitudinal magnetic field using generalized differential quadrature method", *Proc. Inst. Mech. Eng. C. J. Mech. Eng. Sci.* **231**(20), 3866-3885. https://doi.org/10.1177/0954406216653622.

Moradi-Dastjerdi, R. and Behdinan, K. (2019), "Thermoelastic static and vibrational behaviors of nanocomposite thick cylinders reinforced with graphene", *Steel Compos. Struct.*,

31(5), 529-539. https://doi.org/10.12989/scs.2019.31.5.529.

Nanthakumar, S.S., Lahmer, T., Zhuang, X., Zi, G. and Rabczuk, T. (2016), "Detection of material interfaces using a regularized level set method in piezoelectric structures", *Sci. Eng.*, **24**(1), 153-176. https://doi.org/10.1080/17415977.2015.1017485.

Pourjabari, A., Hajilak, Z.E., Mohammadi, A.R., Habibi, M. and Safarpour, H. (2019), "Effect of porosity on free and forced vibration characteristics of the GPL reinforcement composite nanostructures", *Comput. Math. Appl.*, **77**(10), 2608-2626. https://doi.org/10.1016/j.camwa.2018.12.041.

Qin, L., Wang, J., Liu, D., Tang, L. and Song, G. (2019), "Analysis on an improved resistance tuning type multi-frequency piezoelectric spherical transducer", *Smart Struct. Syst.*, **24**(4), 435-446. https://doi.org/10.12989/sss.2019.24.4.435.

Rabczuk, T., Ren, H. and Zhuang, X. (2019), "A nonlocal operator method for partial differential equations with application to electromagnetic waveguide problem", *Compos. Mater.*, **59**(1), 31-55. https://doi.org/10.32604/cmc.2019.04567.

Rahmani, O. and Pedram, O. (2014), "Analysis and modeling the size effect on vibration of functionally graded nanobeams based on nonlocal Timoshenko beam theory", *Int. J. Eng. Sci.*, **77**, 55-70. https://doi.org/10.1016/j.ijengsci.2013.12.003.

Rajabi, J. and Mohammadimehr, M. (2019), "Bending analysis of a micro sandwich skew plate using extended Kantorovich method based on Eshelby-Mori-Tanaka approach", *Comput. Concrete*, **23**(5), 361-376. https://doi.org/10.12989/cac.2019.23.5.361.

Reddy, R.M.R., Karunasena, W. and Lokuge, W. (2018), "Free vibration of functionally graded-GPL reinforced composite plates with different boundary conditions", *Aerosp. Sci. Technol.*, **78**, 147-156. https://doi.org/10.1016/j.ast.2018.04.019.

Rostami, R., Irani Rahaghi, M. and Mohammadimehr, M. (2019), "Vibration control of the rotating sandwich cylindrical shell considering functionally graded core and functionally graded magneto-electro-elastic layers by using differential quadrature method", *J. Sandw. Struct. Mater.*, 1099636218824139. https://doi.org/10.1177/1099636218824139.

Sadighi, M., Benvidi, M.H. and Eslami, M.R. (2011), "Improvement of thermo-mechanical properties of transversely flexible sandwich panels by functionally graded skins", *J. Sandw. Struct. Mater.*, **13**(5), 539–577. https://doi.org/10.1177/1099636211400130.

Sahla, M., Saidi, H., Draiche, K., Bousahla, A.A., Bourada, F. and Tounsi, A. (2019), "Free vibration analysis of angle-ply laminated composite and softcore sandwich plates", *Steel Compos. Struct.*, **33**(5), 663-679. https://doi.org/10.12989/scs.2019.33.5.663.

Sahmani, S. and Mohammadi Aghdam, M. (2018a), "Small scale effects on the large amplitude nonlinear vibrations of multilayer functionally graded composite nanobeams reinforced with graphene-nanoplatelets", *Int. J. Nanosci. Nanotechnol.*, **14**(3), 207-227.

Sahmani, S., Mohammadi Aghdam, M. and Rabczuk, T. (2018b), "Nonlinear bending of functionally graded porous micro/nano-beams reinforced with graphene platelets based upon nonlocal strain gradient theory", *Compos. Struct.*, **186**, 68-78. https://doi.org/10.1016/j.compstruct.2017.11.082.

Sahmani, S., Mohammadi Aghdam, M. and Rabczuk, T. (2018c), "Nonlocal strain gradient plate model for nonlinear large-amplitude vibrations of functionally graded porous micro/nano-plates reinforced with GPLs", *Compos. Struct.*, **198**, 51-62. https://doi.org/10.1016/j.compstruct.2018.05.031

Sankar, B.V. and Tzeng, J.T. (2002), "Thermal stresses in functionally graded beams", *AIAA J.*, **40**(6), 1228-1232. https://doi.org/10.2514/2.1775.

Semmah, A., Heireche, H., Bousahla, A.A. and Tounsi, A. (2019), "Thermal buckling analysis of SWBNNT on Winkler foundation by nonlocal FSDT", *Adv. Nano Res.*, **7**(2), 89-98. https://doi.org/10.12989/anr.2019.7.2.089.

Sheng, G.G. and Wang, X. (2013), "Nonlinear vibration control of functionally graded laminated cylindrical shells", *Compos. B. Eng.*, **52**, 1-10. https://doi.org/10.1016/j.compositesb.2013.03.008.

Shokravi, M. (2018), "Dynamic buckling of smart sandwich beam subjected to electric field based on hyperbolic piezoelasticity theory", *Smart Struct. Syst.*, **22**(3), 327-334. https://doi.org/10.12989/sss.2018.22.3.327.

Şimşek, M. (2019), "Some closed-form solutions for static, buckling, free and forced vibration of functionally graded (FG) nanobeams using nonlocal strain gradient theory", *Compos. Struct.*, **224**, 111041. https://doi.org/10.1016/j.compstruct.2019.111041.

Singh, A.K., Negi, A. and Koley, S. (2019), "Influence of surface irregularity on dynamic response induced due to a moving load on functionally graded piezoelectric material substrate", *Smart Struct. Syst.*, **23**(1), 31-44. https://doi.org/10.12989/sss.2019.23.1.031.

Sobhy, M. (2018), "Magneto-electro-thermal bending of FG-graphene reinforced polymer doubly-curved shallow shells with piezoelectromagnetic faces", *Compos. Struct.*, **203**, 844-860. https://doi.org/10.1016/j.compstruct.2018.07.056.

Tahouneh, V. (2018), "Vibration analysis of sandwich sectorial plates considering FG wavy CNT-reinforced face sheets", *Steel Compos. Struct.*, **28**(5), 541-557. https://doi.org/10.12989/scs.2018.28.5.541.

Thanh, C. V., Tran, L., Bui, T.Q., Nguyen, H.X. and Abdel-Wahab, M. (2019), "Isogeometric analysis for size-dependent nonlinear thermal stability of porous FG microplates", *Compos. Struct.*, **221**, 110838. https://doi.org/10.1016/j.compstruct.2019.04.010.

Tlidji, Y., Zidour, M., Draiche, K., Safa, A., Bourada, M., Tounsi, A., Bousahla, A.A. and Mahmoud, S.R. (2019), "Vibration analysis of different material distributions of functionally graded microbeam", *Struct. Eng. Mech.*, **69**(6), 637-649. https://doi.org/10.12989/sem.2019.69.6.637.

Vu-Bac, N., Lahmer, T., Zhuang, X., Nguyen-Thoi, T. and Rabczuk, T. (2016), "A software framework for probabilistic sensitivity analysis for computationally expensive models", *Adv. Eng. Soft.*, **100**, 19-31. https://doi.org/10.1016/j.advengsoft.2016.06.005.

Wang, L., Haugen, N.O., Wu, Z., Shu, X., Jia, Y., Ma, J., Yu, S., Li, H. and Chai, Q. (2019a), "Ferroelectric BaTiO3@ZnO heterostructure nanofibers with enhanced pyroelectrically-driven-catalysis", *Ceram. Int.*, **45**(1), 90-95. https://doi.org/10.1016/j.ceramint.2018.09.137.

Wang, Y.Q., Liu, Y.F. and Zu, J.W. (2019b), "Analytical treatment of nonlocal vibration of multilayer functionally graded piezoelectric nanoscale shells incorporating thermal and electrical effect", *Eur. Phys. J. Plus*, **134**(2), 54. https://doi.org/54. 10.1140/epjp/i2019-12405-9.

Xiaobai, L., Li, L., Hu, Y., Ding, Z. and Deng, W. (2017), "Bending, buckling and vibration of axially functionally graded beams based on nonlocal strain gradient theory", *Compos. Struct.*, **165**, 250-265. https://doi.org/10.1016/j.compstruct.2017.01.032.

Xiong, Q.l. and Tian, X. (2017), "Transient thermo-piezo-elastic responses of a functionally graded piezoelectric plate under thermal shock", *Steel Compos. Struct.*, **25**(2), 187-196. https://doi.org/10.12989/scs.2017.25.2.187.

Xu, X.J., Wang, X.C., Zheng, M.L. and Ma, Z. (2017), "Bending and buckling of nonlocal strain gradient elastic beams", *Compos. Struct.*, **160**, 366-377. https://doi.org/10.1016/j.compstruct.2016.10.038.

Yang, B., Kitipornchai, S., Yang, Y.F. and Yang, J. (2017), "3D

thermo-mechanical bending solution of functionally graded graphene reinforced circular and annular plates", *Appl. Math. Model.*, **49**, 69-86. https://doi.org/10.1016/j.apm.2017.04.044.

Yang, J., Chen, D. and Kitipornchai, S. (2018a), "Buckling and free vibration analyses of functionally graded graphene reinforced porous nanocomposite plates based on Chebyshev-Ritz method", *Compos. Struct.*, **193**, 281-294. https://doi.org/10.1016/j.compstruct.2018.03.090.

Yang, Y., Yang, B. and Niu, M. (2018b), "Dynamic/static displacement sensor based on magnetoelectric composites", *Appl. Phys. Lett.*, **113**(3), 032903. https://doi.org/10.1063/1.5037378.

Yu, T., Hu, H., Zhang, J. and Quoc Bui, T. (2019), "Isogeometric analysis of size-dependent effects for functionally graded microbeams by a non-classical quasi-3D theory", *Thin Wall. Struct.*, **138**, 1-14. https://doi.org/10.1016/j.tws.2018.12.006.

Yu, T., Zhang, J., Hu, H. and Bui, T.Q. (2019), "A novel size-dependent quasi-3D isogeometric beam model for two-directional FG microbeams analysis", *Compos. Struct.*, **211**, 76-88. https://doi.org/10.1016/j.compstruct.2018.12.014.

Zarga, D., Tounsi, A., Bousahla, A.A., Bourada, F. and Mahmoud, S.R. (2019), "Thermomechanical bending study for functionally graded sandwich plates using a simple quasi-3D shear deformation theory", *Steel Compos. Struct.*, **32**(3), 389-410. https://doi.org/10.12989/scs.2019.32.3.389.

Zeng, S., Wang, B.L. and Wang, K.F. (2019), "Nonlinear vibration of piezoelectric sandwich nanoplates with functionally graded porous core with consideration of flexoelectric effect", *Compos. Struct.*, **207**, 340-351. https://doi.org/10.1016/j.compstruct.2018.09.040.

CC

Appendix A

$$\{A_{11}, B_{11}, P_{11}\} = \sum \int Q_{11r}\{1, z, z^2\}dz_r$$

$$A_{22} = \sum k_s \int Q_{22r}\, dz_r \quad (r = c, tg, bg, tp, bp)$$

$$\{G_e, G_m, S_e, S_m\} = \sum \frac{\pi}{h_p} \int \{e_{113}, q_{113}, ze_{113}, zq_{113}\} sin\left(\frac{\pi \bar{z}_j}{h_p}\right) dz_j$$

$$\{O_e, O_m\} = \sum \int \{e_{131}, q_{131}\} cos\left(\frac{\pi \bar{z}_j}{h_p}\right) dz_j$$

$$\{T_z, \bar{T}_z\} = \sum \frac{\pi}{h_p} \int e_{311}\{1, z\} sin\left(\frac{\pi \bar{z}_j}{h_p}\right) dz_j$$

$$\{R_z, \bar{R}_z\} = \sum \frac{\pi}{h_p} \int q_{311}\{1, z\} sin\left(\frac{\pi \bar{z}_j}{h_p}\right) dz_j$$

$$\{X_e, X_m, \bar{X}_m\} = \sum \int \{g_{11}, \eta_{11}, \beta_{11}\} cos^2\left(\frac{\pi \bar{z}_j}{h_p}\right) dz_j$$

$$\{Y_e, Y_m, \bar{Y}_m\} = \sum \left(\frac{\pi}{h_p}\right)^2 \int \{g_{33}, \eta_{33}, \beta_{33}\} sin^2\left(\frac{\pi \bar{z}_j}{h_p}\right) dz_j \quad (j = tp, bp)$$

$$-\frac{h_c}{2} < z_c < \frac{h_c}{2}$$

$$\frac{h_c}{2} < z_{tg} < \frac{h_c}{2} + h_g$$

$$-\frac{h_c}{2} - h_g < z_{bg} < -\frac{h_c}{2}$$

$$\frac{h_c}{2} + h_g < z_{tp} < \frac{h_c}{2} + h_g + h_p$$

$$-\frac{h_c}{2} - h_g - h_p < z_{bp} < -\frac{h_c}{2} - h_g$$

Appendix B

$$K_{11} = A_{11}\left(\zeta_n{}^2 + \varrho\zeta_n{}^4\right)$$

$$K_{12} = 0$$

$$K_{13} = B_{11}\left(\zeta_n{}^2 + \varrho\zeta_n{}^4\right)$$

$$K_{14} = -G_e\left(\zeta_n + \varrho\zeta_n{}^3\right)$$

$$K_{15} = -G_m\left(\zeta_n + \varrho\zeta_n{}^3\right)$$

$$K_{21} = 0$$

$$K_{22} = -(N^T + N^E + N^M)\left(\zeta_n + \epsilon\zeta_n{}^4\right) + K_1\left(1 + \epsilon\zeta_n{}^2\right) + K_2\left(\zeta_n{}^2 + \epsilon\zeta_n{}^4\right) + A_{22}\left(\zeta_n{}^2 + \epsilon\zeta_n{}^4\right)$$

$$K_{23} = A_{22}\left(\zeta_n + \varrho\zeta_n{}^3\right)$$

$$K_{24} = -O_e\left(\zeta_n{}^2 + \varrho\zeta_n{}^4\right)$$

$$K_{25} = -O_m\left(\zeta_n{}^2 + \varrho\zeta_n{}^4\right)$$

$$K_{31} = B_{11}\left(\zeta_n{}^4 + \varrho\zeta_n{}^4\right)$$

$$K_{32} = A_{22}\left(\zeta_n + \varrho\zeta_n{}^3\right)$$

$$K_{33} = P_{11}\left({\zeta_n}^4 + \varrho{\zeta_n}^4\right) + A_{22}\left(1 + \varrho{\zeta_n}^2\right)$$
$$K_{34} = -(O_e + S_e)\left(\zeta_n + \varrho{\zeta_n}^3\right)$$
$$K_{35} = -(O_m + S_m)\left(\zeta_n + \varrho{\zeta_n}^3\right)$$
$$K_{41} = -T_z\left(\zeta_n + \varrho{\zeta_n}^3\right)$$
$$K_{42} = -O_e\left({\zeta_n}^2 + \varrho{\zeta_n}^4\right)$$
$$K_{43} = -(O_e + \bar{T}_z)\left(\zeta_n + \varrho{\zeta_n}^3\right)$$
$$K_{44} = -X_m\left({\zeta_n}^2 + \varrho{\zeta_n}^4\right)$$
$$K_{45} = -X_e\left({\zeta_n}^2 + \varrho{\zeta_n}^4\right) - Y_e\left(1 + \varrho{\zeta_n}^2\right)$$
$$K_{51} = -R_z\left(\zeta_n + \varrho{\zeta_n}^3\right)$$
$$K_{52} = -O_m\left({\zeta_n}^2 + \varrho{\zeta_n}^4\right)$$
$$K_{53} = -(O_m + \bar{R}_z)\left(\zeta_n + \varrho{\zeta_n}^3\right)$$
$$K_{54} = -X_e\left({\zeta_n}^2 + \varrho{\zeta_n}^4\right) - Y_e\left(1 + \varrho{\zeta_n}^2\right)$$
$$K_{55} = -\bar{X}_m\left({\zeta_n}^2 + \varrho{\zeta_n}^4\right) - \bar{Y}_m\left(1 + \varrho{\zeta_n}^2\right)$$

Appendix C

$$a_1 = \left(\frac{K_{54}}{K_{45}K_{54} - K_{44}K_{55}}\right)\left(\frac{K_{44}}{K_{54}}K_{51} - K_{41}\right)$$
$$a_2 = \left(\frac{K_{54}}{K_{45}K_{54} - K_{44}K_{55}}\right)\left(\frac{K_{44}}{K_{54}}K_{52} - K_{42}\right)$$
$$a_3 = \left(\frac{K_{54}}{K_{45}K_{54} - K_{44}K_{55}}\right)\left(\frac{K_{44}}{K_{54}}K_{53} - K_{43}\right)$$
$$a_4 = -\frac{K_{55}a_1 + K_{51}}{K_{54}}$$
$$a_5 = -\frac{K_{55}a_2 + K_{52}}{K_{54}}$$
$$a_6 = -\frac{K_{55}a_3 + K_{53}}{K_{54}}$$